INFORMATION TO USERS

This reproduction was made from a copy of a document sent to us for microfilming. While the most advanced technology has been used to photograph and reproduce this document, the quality of the reproduction is heavily dependent upon the quality of the material submitted.

The following explanation of techniques is provided to help clarify markings or notations which may appear on this reproduction.

1. The sign or "target" for pages apparently lacking from the document photographed is "Missing Page(s)". If it was possible to obtain the missing page(s) or section, they are spliced into the film along with adjacent pages. This may have necessitated cutting through an image and duplicating adjacent pages to assure complete continuity.

2. When an image on the film is obliterated with a round black mark, it is an indication of either blurred copy because of movement during exposure, duplicate copy, or copyrighted materials that should not have been filmed. For blurred pages, a good image of the page can be found in the adjacent frame. If copyrighted materials were deleted, a target note will appear listing the pages in the adjacent frame.

3. When a map, drawing or chart, etc., is part of the material being photographed, a definite method of "sectioning" the material has been followed. It is customary to begin filming at the upper left hand corner of a large sheet and to continue from left to right in equal sections with small overlaps. If necessary, sectioning is continued again—beginning below the first row and continuing on until complete.

4. For illustrations that cannot be satisfactorily reproduced by xerographic means, photographic prints can be purchased at additional cost and inserted into your xerographic copy. These prints are available upon request from the Dissertations Customer Services Department.

5. Some pages in any document may have indistinct print. In all cases the best available copy has been filmed.

University Microfilms International
300 N. Zeeb Road
Ann Arbor, MI 48106

Edoh, Otto

OPTICAL PROPERTIES OF CARBON FROM THE FAR INFRARED TO THE FAR ULTRAVIOLET

The University of Arizona PH.D. 1983

OPTICAL PROPERTIES OF CARBON FROM THE FAR INFRARED TO THE FAR ULTRAVIOLET

by

Otto Edoh

A Dissertation Submitted to the Faculty of the

DEPARTMENT OF PHYSICS

In Partial Fulfillment of the Requirements
For the Degree of

DOCTOR OF PHILOSOPHY

In the Graduate College

THE UNIVERSITY OF ARIZONA

1 9 8 3

THE UNIVERSITY OF ARIZONA
GRADUATE COLLEGE

As members of the Final Examination Committee, we certify that we have read the dissertation prepared by Otto Edoh

entitled Optical Properties of Carbon from the Far Infrared to the Far Ultraviolet

and recommend that it be accepted as fulfilling the dissertation requirement for the Degree of Doctor of Philosophy.

John W Robertson	Mar 24, 1983
Ke Ching Hsieh	24 Mar. 1983
[signature]	24 Mar 1983
D J Donahue	24 March 1983
[signature]	24 March 1983

Date

Final approval and acceptance of this dissertation is contingent upon the candidate's submission of the final copy of the dissertation to the Graduate College.

I hereby certify that I have read this dissertation prepared under my direction and recommend that it be accepted as fulfilling the dissertation requirement.

Donald R. Huffman — Dissertation Director

24 March 1983 — Date

In memory of my father,

the Rev. Goka H. Edoh,

who made many sacrifices for

the education of his children.

And to my mother,

Naokemi B. Edoh,

whose loving care for her children

has never failed.

STATEMENT BY AUTHOR

This dissertation has been submitted in partial fulfillment of requirements for an advanced degree at The University of Arizona and is deposited in the University Library to be made available to borrowers under rules of the Library.

Brief quotations from this dissertation are allowable without special permission, provided that accurate acknowledgment of source is made. Requests for permission for extended quotation from or reproduction of this manuscript in whole or in part may be granted by the head of the major department or the Dean of the Graduate College when in his judgment the proposed use of the material is in the interests of scholarship. In all other instances, however, permission must be obtained from the author.

SIGNED: 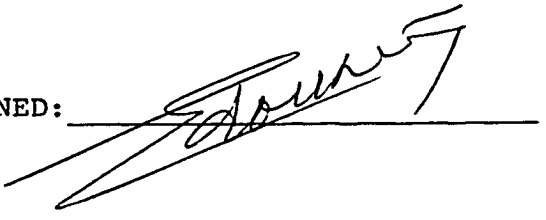

ACKNOWLEDGMENTS

I would like to express my deep gratitude to Dr. Donald R. Huffman, my advisor, who led me with patience and competence to the successful completion of this dissertation. With exceptional skill at motivating students, Dr. Huffman has often refueled my enthusiasm for my research which sometimes seemed hopeless. My debt to him is huge.

Dr. Arlon J. Hunt, of the Lawrence Berkeley Laboratory, allowed me to take my research topic from one of his projects. He provided me with carbon particle samples and constantly shared information with me. I also spent one month working in his laboratory. For all this and for prospects of future collaboration, I am grateful.

My appreciation goes to the members of my examination committee: Dr. Douglas J. Donahue, Dr. Chiang Ke Hsieh, and Dr. John W. Robson. Special thanks are due to Dr. John O. Kessler and to Dr. Richard A. Young, whose generous help during the last part of this work made it possible for me to finish my degree sooner than I could have without them.

Dr. John O. Stoner kindly provided me with carbon foil samples with which I started my research. Dr. Bruce R. Barrett and Dr. Michael D. Scadron have shown a constant friendship for which I am grateful. The list would be too

long to name the many people who have helped in one way or another. The faculty, the staff, in brief, the Department of Physics as a whole, has been very supportive and made me feel at home.

Many former graduate students, now respected Ph.D.'s, and fellow graduate students have been instrumental in the successful completion of my graduate studies. Lin Oliver and Kent Pflibsen of our laboratory helped in many ways; their collaboration is appreciated very much. Special thanks are due to Dr. Jan Rathmann who coached me at the laboratory and to whom I channeled the "dumb" questions I did not want to ask my advisor. As Lin put it, "What can we do without Jan?"

Dr. Dan Morrison and Dr. Niranjan Sandesara helped me through the early stages of my graduate work. The friendship of Dr. Peter Rathmann, Dr. Ralph Ballard, Dr. Randy Bos, Keith Krueger, and Fouad Jalbout has been most beneficial.

I am indebted to my wife's parents, Afiavi and Atone Abalo, and to her brothers, for their understanding and for the support they gave my wife and children before they joined me in Tucson. Thanks are also due to my brothers and sisters for their encouragement and especially to Pierre Koffi Edoh, M.D., for his financial support.

Henri and Nadia have spent many evenings and weekends without their "daddy." Melissa appeared in time to brighten

the dark side of writing my dissertation. For your contribution, "Papa" says thanks.

My wife, Malalasoa, has lived through the frustrations of graduate studies with me. For her patience, her encouragement, and her support, I owe her my deepest gratitude. Thanks, Malala, for helping me through.

Barbara Bickel's help was invaluable in preparing this manuscript.

The sponsorship and the financial support of the African American Institute and of the government of my country (Togo , West Africa) is gratefully acknowledged.

This work was supported in part by a grant from the Department of the Army.

TABLE OF CONTENTS

TABLE OF CONTENTS--Continued

LIST OF ILLUSTRATIONS

LIST OF ILLUSTRATIONS--Continued

LIST OF TABLES

ABSTRACT

Optical properties of carbon are studied in bulk state from $\lambda \sim 0.05$ to 100 μm for graphite, and from $\lambda \sim 0.05$ to 1000 μm for glassy carbon; in small particle state, the optical studies cover the spectral range going from $\lambda \sim 0.1$ to 100 μm for all the materials.

A Kramers-Kronig analysis of near normal reflectance data and/or a reflectance data fit to a Drude-Lorentz model gave bulk optical constants. These optical constants are used in theoretical calculations of extinction and the results compared with experimental results obtained from measurements of a variety of carbon particles. It is inferred that the high experimentally observed extinction is mainly due to a shape effect.

CHAPTER 1

INTRODUCTION

Optical properties of small particles have become important for a variety of reasons. For example, atmospheric scientists are concerned with the effects of small particles on weather. It is known that the role of atmospheric aerosols in the earth's heat balance depends on their absorptivity and scattering properties (National Academy of Sciences, 1975). In order to predict accurately whether the warming tendency due to absorption and the cooling tendency due to backscattering in the earth's atmosphere will dominate, it is necessary to understand the optical properties of aerosol particulates (Twomey and Huffman, 1982).

The optical properties of small particles are important in astrophysics. The astrophysicist needs to understand the extinction by small particles in order to infer the nature of the solid grains responsible for the observed interstellar absorptions (Huffman, 1977).

Two further examples demonstrate the great diversity of applications of small particles. For military applications, it is desirable to understand the optical properties of particles which are to be used to generate smoke clouds for obscuration of laser weapons and surveillance devices;

for certain solar energy collector types, it has been shown that the energy collection is enhanced by doping the working fluid with very small absorbing particles (Hunt, 1980).

In applications of the later kinds, it is necessary to maximize the absorption by small particles. Thus carbon is a prime candidate material. For example, Abdelrahman, Fumeaux, and Suter (1979) have chosen graphite particles as ideal for suspension in the gas of a solar receiver. Hunt (1978, 1979) has designed a collector-heat exchanger which will utilize carbon particles suspended in air.

The extinction by small particles can be calculated for certain shapes if the optical constants as a function of wavelength are known. Although the literature on optical constants of carbon is abundant, the information is disparate and confined to limited spectral regions. Workers rarely agree with one another in their results. (See Twitty and Weiman, 1971 for a review.)

In this study, two carbonaceous materials, graphite and glassy carbon, chosen because they are well defined (and thus reproducible), are discussed. Graphite is the crystal form, and glassy carbon appears to be the best defined carbon variety close to ideally amorphous carbon.

Definitions and concepts which are dealt with in this work are covered in Chapter 2. In Chapter 3, optical constants of graphite and glassy carbon are surveyed; reflectance data of these materials are compiled from the

literature and augmented by our own measurements and/or extrapolations. The data are analyzed to yield optical constants over a broad spectral range. In Chapter 4, extinction by fine particles and smoke of carbon is experimentally measured, and results compared to theoretical calculations done with the use of the measured optical constants.

CHAPTER 2

REVIEW OF CONCEPTS AND DEFINITIONS

This chapter establishes the notation, defines the optical constants and summarizes the theories which will be used in this work.

After defining the optical constants of solids and showing their relation to the dielectric constant, the classical dispersion relations and the Kramers-Kronig relations are reviewed. The extinction by small particles are introduced through the Mie theory for spheres which leads to the Rayleigh approximations. Rayleigh theory for ellipsoids, and its generalization to the distributions of ellipsoidal shape, are then discussed. Finally, a sum rule for small particle extinction is introduced.

Complex Index of Refraction; Relation to the Complex Dielectric Constant*

Optical properties of solids deal with the interaction of electromagnetic radiation with solid matter. This interaction is described by wavelength dependent complex index of refraction:

$$m(\lambda) = n + i\,k \quad , \tag{1}$$

---

*For a detailed treatment, see any E & M text, Jackson (1975) for example.

where n is the real index of refraction and k the index of absorption. n and k are related to the complex dielectric function ε through the relation:

$$m^2 = (n + ik)^2 = \varepsilon \quad .$$

From $\varepsilon = \varepsilon_1 + i\varepsilon_2$ it follows that:

$$\varepsilon_1 = n^2 - k^2 \tag{2}$$

$$\varepsilon_2 = 2nk \quad . \tag{3}$$

The (n,k) or $(\varepsilon_1,\varepsilon_2)$ pair describes completely the optical properties of a material, but they cannot be directly measured by experiment. The experimental connection is made through the reflectance:

$$R = \left|\frac{E_r}{E_i}\right|^2 = |r|^2$$

where r, the reflectivity coefficient, is a complex function, defined at the surface of a solid, as the ratio of the reflected electric field E_r to the incident electric field E_i. At normal incidence:

$$r = \frac{(n-1) + ik}{(n+1) + ik} \tag{4}$$

and

$$R = \frac{(n-1)^2 + k^2}{(n+1)^2 + k^2} \quad . \tag{5}$$

Dispersion Relations

Classical Dispersion Relations*

The classical theory of absorption was developed by Lorentz (for insulators) and Drude (for free electron metals). The combined use of the two models yields:

$$\varepsilon = 1 - \frac{\omega_p^2}{\omega^2 + i\gamma\omega} + \sum_j \frac{\omega_{pj}^2}{\omega_j^2 - \omega^2 - i\gamma_j\omega}$$

which is equivalent to

$$\varepsilon_1 = 1 - \frac{\omega_p^2}{\omega^2 + \gamma^2} + \sum_j \frac{\omega_{pj}^2(\omega_j^2-\omega^2)}{(\omega_j^2-\omega^2)^2 + \gamma_j^2\omega^2} \qquad (6)$$

$$\varepsilon_2 = \frac{\gamma\omega_p^2}{\omega(\omega^2 + \gamma^2)} + \sum_j \frac{\omega_{pj}^2\,\omega\gamma_j}{(\omega_j^2-\omega^2)^2 + \gamma_j^2\omega^2} \quad , \qquad (7)$$

where ω_j, γ_j and ω_{pj} are respectively the resonance frequency, the damping constant and the plasma frequency of the j^{th} oscillator. They determine the position, the width and the strength of the j^{th} oscillator. The terms out of the summation signs are the Drude terms. The summation is over the number of oscillators. In more compact form (6) and (7) become:

$$\varepsilon_1 = 1 + \sum_j \frac{\omega_{pj}^2(\omega_j^2-\omega^2)}{(\omega_j^2-\omega^2)^2 + \gamma_j^2\omega^2} \quad , \qquad (8)$$

---

*For more information, see for example Wooten (1972, Ch. 3).

$$\varepsilon_2 = \sum_j \frac{\omega_{pj}^2 \, \omega\gamma_j}{(\omega_j^2-\omega^2)^2 + \gamma_j^2\omega^2} \quad . \tag{9}$$

The Drude terms are obtained from (8) and (9) by assuming that the resonance peak of the first oscillator is at zero frequency ($\omega_{j=1} = 0$).

This multiple oscillator model is used in the determination of optical constants of solids. From a reflectance curve, the first values of the parameters ω_j, γ_i and ω_{pj} are found for each peak by locating its position, and determining its width and its strength. They are used in equations (8) and (9) to calculate $\varepsilon_1(\lambda)$ and $\varepsilon_2(\lambda)$ which, by the use of equations (2) and (3) yield $n(\lambda)$ and $k(\lambda)$; the n and k obtained are used in (5) to yield the reflectance. The parameters are varied until the calculated reflectance fits the measured reflectance as well as desired, giving the corresponding $\varepsilon_1(\lambda)$ and $\varepsilon_2(\lambda)$ or $n(\lambda)$ and $k(\lambda)$.

This technique is still valid even if the solid is anisotropic. In this case, the sample has to be well oriented and polarized light must be used.

The Kramers-Kronig Relations*

The reflectivity coefficient can be written as:

$$r(\omega) = \rho(\omega) \, e^{i\theta} \quad . \tag{10}$$

(10)

---

*See for example Wooten (1972, Ch. 6 and Appendix G).

Equating the real parts and the imaginary parts of (4) and (6) leads to:

$$n = \frac{1 - \rho^2}{1 + \rho^2 - 2\rho \cos \theta} , \tag{11}$$

$$k = \frac{2\rho \sin \theta}{1 + \rho^2 - 2\rho \cos \theta} . \tag{12}$$

The knowledge of the phase θ will allow the calculation of n and k. The determination of θ can be done through the use of the Kramers-Kronig relations, which connect the real and imaginary parts of the response function of a linear system. The response function must have the following characteristics:

It has to be frequency dependent.

It has to be causal.

It has to be analytic in the upper half of the complex ω plane.

It can be shown that the reflectivity coefficient is a response function between the incident and reflected wave at the surface of a solid. It can also be shown that

$$\ln r(\omega) = \ln \rho(\omega) + i\theta(\omega)$$

satisfies the requirements for the application of the Kramers-Kronig relations.

The relation between $\theta(\omega)$ and $\rho(\omega)$ which is of interest in this treatment is:

$$\theta(\omega) = -\frac{2\omega}{\pi} P \int_0^\infty \frac{\ln \rho(\omega')}{\omega'^2 - \omega^2} d\omega' \quad ,$$

where P is a principal part. The removal of the principal part and the replacement of $\rho(\omega')$ by $|R(\omega')|^{\frac{1}{2}}$ gives:

$$\theta(\omega) = \frac{\omega}{\pi} \int_0^\infty \frac{\ln [R(\omega')/R(\omega)]}{\omega^2 - \omega'^2} d\omega' \quad .$$

In terms of wavelength, the substitution of $\omega = 2\pi c/\lambda$ can be made to yield:

$$\theta(\lambda) = \frac{2\lambda}{\pi} \int_0^\infty \frac{\ln [R(\lambda')/R(\lambda)]}{\lambda'^2 - \lambda^2} d\lambda' \quad . \tag{13}$$

Relation (13) suggests that the reflectance has to be measured from zero to infinite wavelength. This is impossible in practice; in general, the reflectance is measured for λ such that:

$$\lambda_{min} \leq \lambda \leq \lambda_{max} \quad .$$

Thus, (13) can be rewritten:

$$\theta(\lambda) = \frac{2\lambda}{\pi} \int_0^{\lambda_{min}} \frac{\ln [R(\lambda')/R(\lambda)]}{\lambda'^2 - \lambda^2} d\lambda'$$

$$+ \frac{2\lambda}{\pi} \int_{\lambda_{min}}^{\lambda_{max}} \frac{\ln [R(\lambda')/R(\lambda)]}{\lambda'^2 - \lambda^2} d\lambda' + \frac{2\lambda}{\pi} \int_{\lambda_{max}}^\infty \frac{\ln [R(\lambda')/R(\lambda)]}{\lambda'^2 - \lambda^2} d\lambda'$$

$$= \theta_1(\lambda) + \theta_2(\lambda) + \theta_3(\lambda) \quad .$$

θ_2 is calculated with the actual experimental data. For $\theta_1(\lambda)$ and $\theta_3(\lambda)$, some sort of extrapolation has to be done. For metal and metal-like materials, the Drude model can be used to find $R(\lambda')$ and compute $\theta_3(\lambda)$. For other kinds of materials, Steyer (1974) derived a relation based on the classical dispersion theory.

The short wavelength spectral range is more difficult to treat. To include all the interband transitions, the reflectance is approximated by:

$$R(\lambda) = R_{le} \times (\lambda/\lambda_{le})^{s} \quad , \tag{14}$$

where $\lambda < \lambda_{le}$ and $s > 0$. R_{le} and λ_{le} are the reflectance and the wavelength at the last experimental point. At lower wavelengths, the reflectance is approximated by:

$$R(\lambda) = R_f \times (\lambda/\lambda_f)^{4} \quad . \tag{15}$$

R_f is calculated by the use of (14) at the point where the second extrapolation starts.

With this extrapolation, it is assumed that the wavelength is low enough to allow a free-electron description of the electrons.

These extrapolations are used in the integration of $\theta_1(\lambda)$ to yield (Wooten, 1972, p. 249):

$$\theta_1(\lambda) = \frac{1}{2\pi} \ln\left[\frac{R_f}{R(\lambda)}\right] \ln\left[\frac{|\lambda-\lambda_{1e}|}{\lambda+\lambda_{1e}}\right] + \frac{1}{\pi} \sum \left[s \frac{(\lambda_{1e}/\lambda)^{2n+1}}{(2n+1)^2} + (4-s) \frac{(\lambda_f/\lambda)^{2n+1}}{(2n+1)^2} \right] . \quad (16)$$

The parameter s and the wavelength λ_f are chosen such that the calculated optical constants are in agreement with those obtained from an independent measurement in a limited spectral range.

The actual reflectance data and the extrapolations are used in the numerical integration which is done by the use of Simpson's rule of integration.

Extinction by Small Particles

Introduction to Mie Theory

A beam of light which passes through a collection of particles is attenuated. This attenuation, due to scattering and absorption by the particles, is called extinction which is defined to be:

$$\text{Extinction} = \text{Scattering} + \text{Absorption} .$$

A way for inferring the extinction is to calculate the transmission T of the beam through a path length ℓ of the distribution of particles. For N spherical particles per unit volume, each of radius a:

$$T = I/I_o = \exp(-NQ_{ext}\pi a^2)\ell \quad , \tag{17}$$

where:

$$Q_{ext} = Q_{sca} + Q_{abs} \quad .$$

The Q's are called efficiency factors for spheres, and are related to the following quantities:

$C_{sca} = Q_{sca}\,\pi\,a^2$ is the cross section for removal of energy from the incident beam by scattering,

$C_{abs} = Q_{abs}\,\pi\,a^2$ is the cross section for removal of energy from the incident beam by absorption,

$$C_{ext} = C_{sca} + C_{abs} \quad . \tag{18}$$

Mie (1908) and Debye (1909) developed a theory for calculating the efficiency factors for spheres of arbitrary sizes. This theory, usually referred to as the Mie theory is presented in books by van de Hulst (1957), Kerker (1969) and Bohren and Huffman (1983).

From the theory:

$$Q_{sca} = \frac{2}{x^2} \sum_{n=1}^{\infty} (2n+1)\,[|a_n|^2 + |b_n|^2] \quad , \tag{19}$$

$$Q_{abs} = \frac{2}{x^2} \sum_{n=1}^{\infty} (2n+1)\,\mathrm{Re}(a_n + b_n) \quad , \tag{20}$$

where $x = 2\pi a/\lambda$ is the size parameter. The coefficients a_n and b_n are complex expressions involving spherical Bessel and Hankel functions and their derivatives. They can be computed for given values of the complex index of refraction

n and the size parameter x. The computation procedure is given by Wichramasinghe (1973) and related computer programs are in the book by Bohren and Huffman (1983).

Theory and experiment are connected as follows. If we define:

$$N = n/V \quad ,$$

where n is the total number of particles in the volume V,

$$C = m/V = \frac{n}{V}\frac{4}{3}\pi a^3 \rho \quad ,$$

where m is the total mass of particles and ρ the mass density of the particle material, (17) becomes:

$$I/I_o = \exp\left(-\alpha \frac{C\ell}{\rho}\right)$$

$$= \exp\left(-\alpha \frac{\sigma}{\rho}\right) \quad , \tag{21a}$$

$$\alpha = \frac{\rho}{\sigma} \ln\left(I_o/I\right) \quad . \tag{21b}$$

If the optical density (O.D.) defined as: $O.D. = \frac{1}{2.3} \ln \frac{I_o}{I}$ is used, then $\alpha = 2.3 \frac{\rho}{\sigma} (O.D.)$, where σ is the mass/area of particles. Also

$$\alpha = \frac{Q_{ext}\pi a^2}{4/3\,\pi a^3} = \frac{3}{4}\frac{Q_{ext}}{a} \quad . \tag{22}$$

α is the volume normalized extinction coefficient and is related to the mass extinction coefficient α_p by:

$$\alpha_p = \frac{\alpha}{\rho} \quad . \tag{23}$$

In the case of a size distribution of spheres:

$$\alpha = \frac{\int N(a)Q(a)\pi a^3 da}{\int N(a)\,\frac{4}{3}\pi a^3\,da} \quad ,$$

where N(a) is the number of particles per unit volume with radii varying between a and a + da.

From (21), α can be determined experimentally by measuring the transmission and σ. The use of (22) leads to an experimental value of Q_{ext}.

If the particles are very small compared to the wavelength ($a << \lambda$) and when the phase shift of light in the particle is negligible ($|m|x << 1$) (Rayleigh approximation), then the Mie efficiency factors can be expanded in power series as functions of the size parameter x; the lowest power terms of importance in a first approximation are:

$$Q_{sca} = \frac{8}{3} x^4 \left| \left(\frac{m^2-1}{m^2+2} \right) \right|^2 \quad , \tag{24}$$

$$Q_{abs} = 4\, x\, \mathrm{Im} \left\{ \frac{m^2-1}{m^2+2} \right\} \quad . \tag{25}$$

Relations (24) and (25) apply when the particles are in a medium with complex index of refraction $m'^2 = 1$. They can be generalized to give:

$$Q_{sca} = \frac{8}{3} x^4 \left| \left(\frac{\varepsilon-\varepsilon_m}{\varepsilon+2\varepsilon_m} \right) \right|^2 \quad , \tag{26}$$

$$Q_{abs} = 4\, x\, \mathrm{Im} \left\{ \frac{\varepsilon-\varepsilon_m}{\varepsilon+2\varepsilon_m} \right\} \quad , \tag{27}$$

where ε is the dielectric constant of the particles and ε_m is the dielectric constant of the medium in which they are embedded.

The Rayleigh approximations have introduced two main simplifications in the treatment of extinction by small particles. First of all, there is no shape effect in volume normalized extinction, as illustrated in Fig. 2.1. At small radii, the extinction is a constant. However, for radii above 0.012 μm, the extinction is extremely radius dependent. One notices a decrease in extinction for radius larger than 0.1 μm. This decrease is due to saturation effect; when absorption is very effective, the inner parts of the sphere do not participate in the absorption process. With larger spheres, more of the inner volume is ineffective, which results in a decrease of the extinction per unit volume.

From an experimental point of view, one does not have to worry about the size distribution of particles if they are small enough compared to the wavelength. This occurs easily in the IR spectral range.

The second simplification introduced by the Rayleigh approximations is that the shape effects can be more easily treated theoretically, as will be shown in the next section.

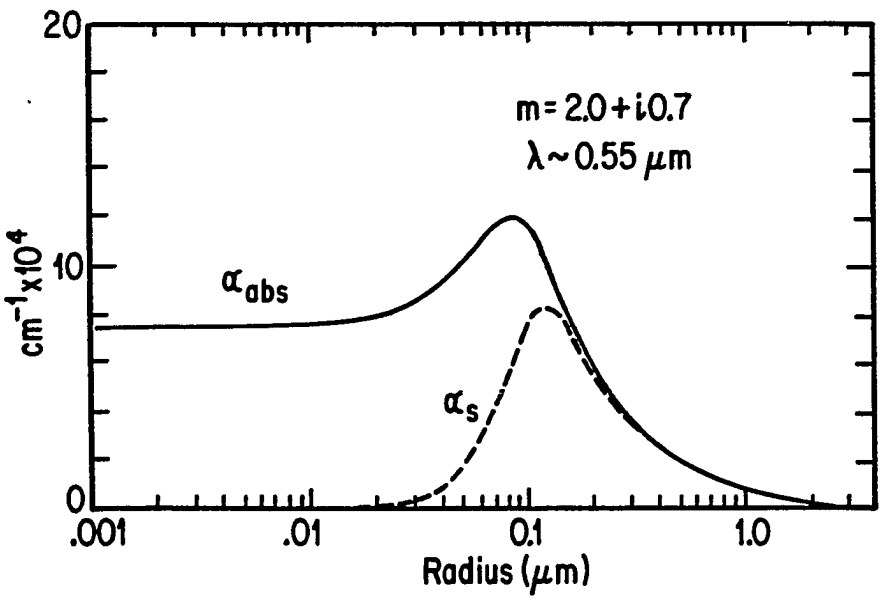

Fig. 2.1. Absorption and scattering cross sections normalized per unit volume of solid for carbon in the visible, calculated using Mie theory.

Rayleigh Theory for Ellipsoids;
The Shape Distribution

Small particles have been discussed with the assumption that they are spherical. Although this is not very often true, the spherical hypothesis allowed the use of the Mie theory which can be generalized to infinite cylinders only. A more realistic shape for particles is the ellipsoid, for which polarizability in an electric field can be determined and used in the derivation of an approximate expression for the absorption and scattering cross-sections, if the Rayleigh conditions are valid. The derivation of the polarizability can be found in the bibliography given for the Mie theory.

For an ellipsoidal particle with semi-axes a, b and c in an electric field parallel to the j^{th} axis $(j = 1,2,3)$, polarizability is given by:

$$\alpha_j = \frac{V}{4\pi} \frac{\varepsilon-\varepsilon_m}{\varepsilon_m + L_j(\varepsilon-\varepsilon_m)} \quad , \tag{28}$$

where $V = (4/3)\pi$ abc is the volume of the ellipsoid. The depolarization factors L_j are given by:

$$L_1 = \frac{abc}{2} \int \frac{ds}{(s+a^2)\ \{(a^2+s)(b^2+s)(c^2+s)\}^{\frac{1}{2}}} \quad , \tag{29}$$

where:

$$s = a + b + c \quad .$$

L_2 and L_3 are computed the same way, with the right substitution in (29). Using the integrals by which the L_j's are calculated, it can be shown that:

$$\sum_{j=1}^{3} L_j = 1 \quad . \tag{30}$$

In the Rayleigh approximations, C_{sca} and C_{abs} for a single ellipsoid of abitrary L_j are:

$$C_{sca}^{j} = \frac{k^4}{6\pi} V^2 \left| \frac{\varepsilon-\varepsilon_m}{\varepsilon_m + L_j(\varepsilon-\varepsilon_m)} \right|^2 \quad , \tag{31}$$

$$C_{abs}^{j} = kV \, \mathrm{Im} \left\{ \frac{\varepsilon-\varepsilon_m}{\varepsilon_m + L_j(\varepsilon-\varepsilon_m)} \right\} \quad . \tag{32}$$

The superscript j shows that E field is parallel to the j^{th} axis; $k = 2\pi/\lambda$. For a collection of ellipsoids randomly oriented, an average value is taken; the absorption case is given:

$$\langle C_{abs} \rangle = \frac{V}{3} k \sum_{j=1}^{3} \frac{\varepsilon_m \varepsilon_2}{L_j\{[\varepsilon_1+\varepsilon_m(1/L_j-1)]^2 + \varepsilon_2^2\}} \, . \tag{33}$$

From (33) it can be seen that resonance occurs when:

$$L_j\varepsilon_1 + \varepsilon_m(1-L_j) = 0$$

or

$$\varepsilon_1 = -\varepsilon_m(1/L_j - 1) \quad . \tag{34}$$

Since $0 \leq L_j \leq 1$, the resonance occurs only for negative values of ε_1. For spheres, $L_j = 1/3$ for all directions, and the resonance is obtained for:

$$\varepsilon_1 = -2\varepsilon_m \quad .$$

A distribution of identical ellipsoids with arbitrary L_j's will give three absorption peaks because of the three values of L_j.

A more general treatment of the preceding case is done by considering a variety of shapes of ellipsoids.

Given a shape distribution expression $P(L_1,L_2)$, it is possible to compute:

$$\langle\langle C_{abs} \rangle\rangle = \iint P(L_1,L_2) \langle C_{abs} \rangle \, dL_1 \, dL_2 \quad . \tag{35}$$

The integration is done over L_1 and L_2 only since from (30) it is seen that only two L_j's are independent.

Assuming that all shapes of ellipsoids are equally probable, which mathematically means that $P(L_1,L_2)$ is a constant, Huffman and Bohren (1980) found (35) to be:

$$\langle\langle C_{abs} \rangle\rangle = k\langle V \rangle \, \mathrm{Im}\left[\frac{2\varepsilon\varepsilon_m}{\varepsilon-\varepsilon_m} \log\left(\varepsilon/\varepsilon_m\right)\right] \quad . \tag{36}$$

(For the log calculation, use $|\varepsilon|$ and $-\pi < \theta < \pi$.) For this treatment, a system of particles with all shapes of ellipsoids should produce absorption over the whole spectral range where ε_1 is negative. Rathmann (1981, p. 18) calculated aluminum absorption coefficients for spheres, single ellipsoids and a continuous distribution of ellipsoids.

Relation (36) is used in our theoretical calculations, and the corresponding curves are labeled CDE (continuous distribution of ellipsoids).

Sum Rule for Extinction

Bohren and Huffman (1983) have derived a sum rule for extinction by spherical particles:

$$\int_0^\infty C_{ext}(\lambda)\, d\lambda = 4\pi^3 a^3 \frac{\varepsilon(\lambda=\infty)+1}{\varepsilon(\lambda=\infty)+2} \quad . \tag{37}$$

For conducting materials, $\varepsilon(\lambda=\infty)$ is large; thus (37) has an upper limit such that:

$$\int_0^\infty C_{ext}(\lambda)\, d\lambda \leq 4\pi^3 a^3 \quad . \tag{38}$$

Using (22) in conjunction with $C_{ext} = Q_{ext}\, \pi^2 a^2$ gives:

$$C_{ext}(\lambda) = \frac{4}{3}\pi a^3\, \alpha(\lambda) \quad . \tag{39}$$

A substitution of (39) in (38) leads to:

$$\int_0^\infty \alpha(\lambda)\, d\lambda \leq 3\pi^2 \quad . \tag{40}$$

This relation will be used to check the sphericity of experimentally produced particles.

The sum rule (37) was first derived by Purcell (1969) for spheroidal particles.

CHAPTER 3

BULK OPTICAL CONSTANTS

Carbon is the generic designation of a large variety of carbonaceous materials including graphite and amorphous carbon. Graphite and amorphous carbon are well defined, but many types of coal and soot differ in composition and structure. According to Dalzell and Sarofin (1969), soots are randomly mixed graphitic particles in a matrix of amorphous carbon; they differ from one another by their hydrogen/carbon ratio. The actual difference in the composition of carbonaceous materials, and apparent differences resulting from the use of inappropriate experimental technique in the determination of the optical constants, have led to results, which in some cases, are hardly comparable. Disagreements in results are shown through the review of some previous work presented below. The large variation in published optical constants can be seen in Fig. 3.1.

Stull and Plass (1960) derived dispersion relations for carbon, which they used to fit some other workers' reflectance data between $\lambda \sim 0.436$ μm and 13 μm. The same method has been used by Dalzell and Sarofin (1969) to fit soot pellet reflectance data in about the same spectral

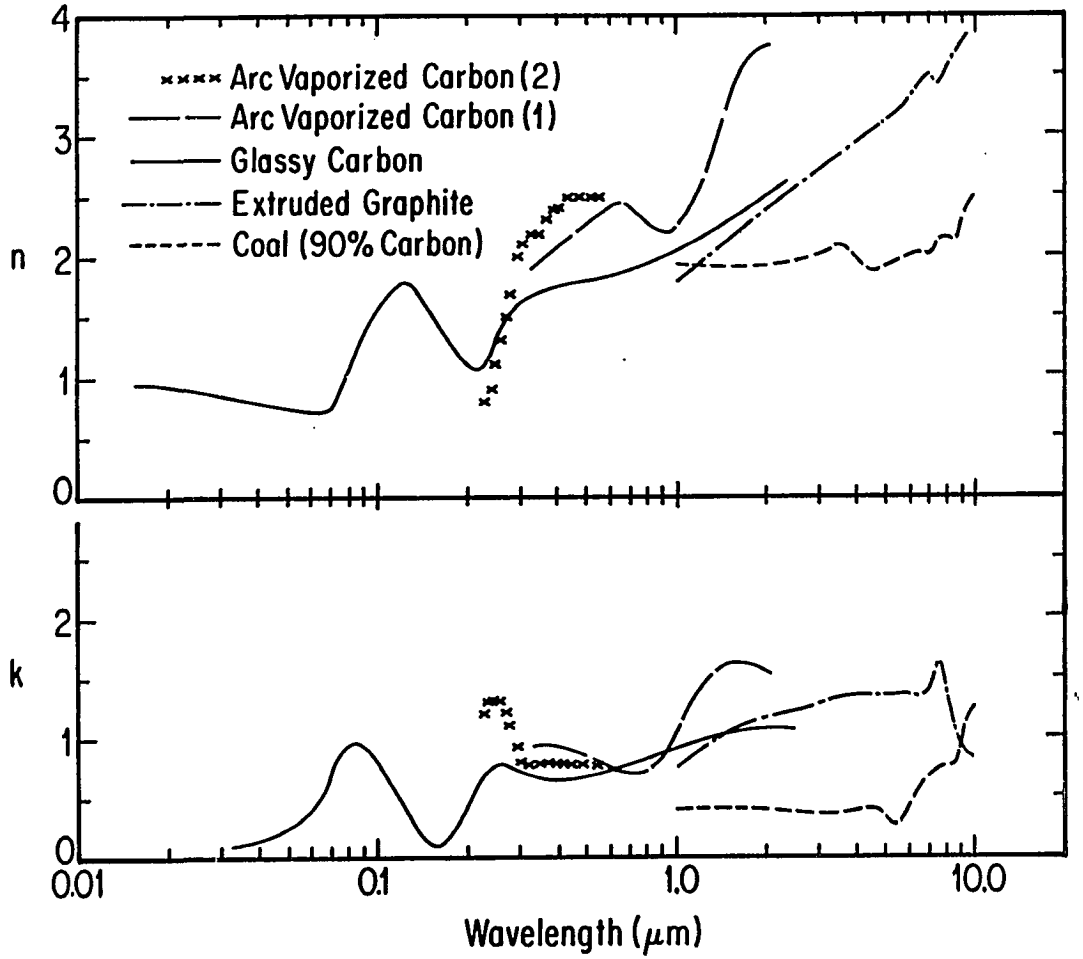

Fig. 3.1. Optical constants n and k for amorphous carbon.

Glassy carbon (Williams and Arakawa, 1972), arc vaporized carbon (Arakawa et al., 1977 for (1) and DiNardo and Goland, 1971 for (2)), extruded graphite and coal (Foster and Howarth, 1968).

range. The results of the two groups do not agree with one another. More recently, Lee and Tien (1981) derived a dispersion model based on electronic band structure considerations. The dispersion constants were determined from the transmission data of soot flame. They questioned their predecessors' methods and results. Tomaselli et al. (1981) measured reflectance of pressed pellets of various carbonaceous materials. They graphically analyzed data by plotting iso-reflectance curves and reading n and k from published tables. None of their results came close to published results for similar materials. DiNardo and Goland (1971) derived optical constants of arc evaporated carbon film by matching the transition radiation theory to experiments from $\lambda \sim 0.23$ μm to 0.56 μm. Arakawa, Williams, and Inagaki (1977) studied a similar material from $\lambda \sim 0.33$ μm to 2.1 μm. A comparison of the two results shows a clear disagreement (see Fig. 3.1). According to Arakawa et al. (1977), the optical properties of arc evaporated carbon vary with the conditions of preparation of the film. Pluchino et al. (1980) isolated a single micro-sized particle of carbon; they electrostatically suspended and irradiated it with a laser beam. The scattered radiation intensity was measured as a function of angle. Electron-microscopy showed that the particle was spherical. Data were then analyzed with the Mie theory. At $\lambda \sim 0.48$ μm and for a particle radius $a \cong 3.06$ μm, n and k are found to be 1.7 and 0.8 respectively.

This review along with Fig. 3.1 has shown that there is no general consensus on optical constants of carbon; it has shown also that available optical constants are confined to a limited spectral range.

In this section, we survey the optical constants of graphite and glassy carbon, and gather existing reflectance data on these materials. In order to calculate the optical constants over a wide spectral range, the reflectance information gathered is completed by our measurements and/or extrapolations wherever it is necessary, to yield a reflectance curve over a wide spectral range, for use in the Kramers-Kronig analysis. A fit of the reflectance data, based on the combined use of Drude and Lorentz dispersion relations has also been done.

Techniques for the determination of optical constants are given; then graphite and glassy carbon are studied in turn.

Techniques for Measuring Optical Constants

Optical properties of solids are due to the wavelength dependence of n and k (ε_1 and ε_2) which cannot be measured directly experimentally. The techniques used to collect information leading to optical constants are summarized in Table 3.1.

Table 3.1. Techniques for determining optical constants of solids.

From Huffman (1977).

Technique	Comments
Transmission methods	
(1) n from minimum deviation; k from transmission and n	High accuracy for n
(2) n and k from transmission and normal incidence reflectance measurements	Easy but useful only in relatively transparent regions
Reflection methods	
(1) Two polarized reflectance measurements at one oblique incidence angle	Larger sample sizes required
(2) Two reflectance measurements at different angles	
(3) Determination of special angles (i.e., Brewster's angle) and reflectance there	
(4) Determination of ellipsometric parameters	Sensitive to surface films
(5) Reflectance in a broad wavelength range and Kramers-Kronig analysis	Extrapolation to 0 and to ∞ necessary
(6) Reflectance vs. wavelength and oscillator model fit to the data	Compact presentation of results as oscillator parameters
Other methods	
(1) Electron energy loss measurements	Does not require polished surfaces

Graphite

Perfect graphite crystals are rare. Figure 3.2 represents the ideal natural graphitic structure. The basal planes are such that every other plane fits exactly over the first; this is the ABAB arrangement. Another one is such that the basal planes are in the ABCABC sequence.

The atoms of carbon are associated in hexagonal rings. Each atom has four electrons on its outer shell; three of them (σ-electrons) participate in holding together the hexagonal ring by covalent bonds; the fourth one (π-electron) moves in the ring and contributes to the bonding between planes. Many properties of graphite, including its optical properties, are highly anisotropic. The anisotropy of the optical properties is due to the ease with which the π-electrons move in the layer planes; higher energy is needed to jump from plane to plane.

Forms most closely approaching the ideal structure of the material graphite are pyrolytic graphite and annealed pyrolytic graphite. Pyrolytic graphite is produced by a decomposition of a hydrocarbon on a hot surface. Although it is not a true graphite, its properties are extremely anisotropic. It can be converted into almost perfect single crystals by heating at temperatures above 2900°C for several hours. It is then called (stress) annealed pyrolytic graphite (Shobert, 1964).

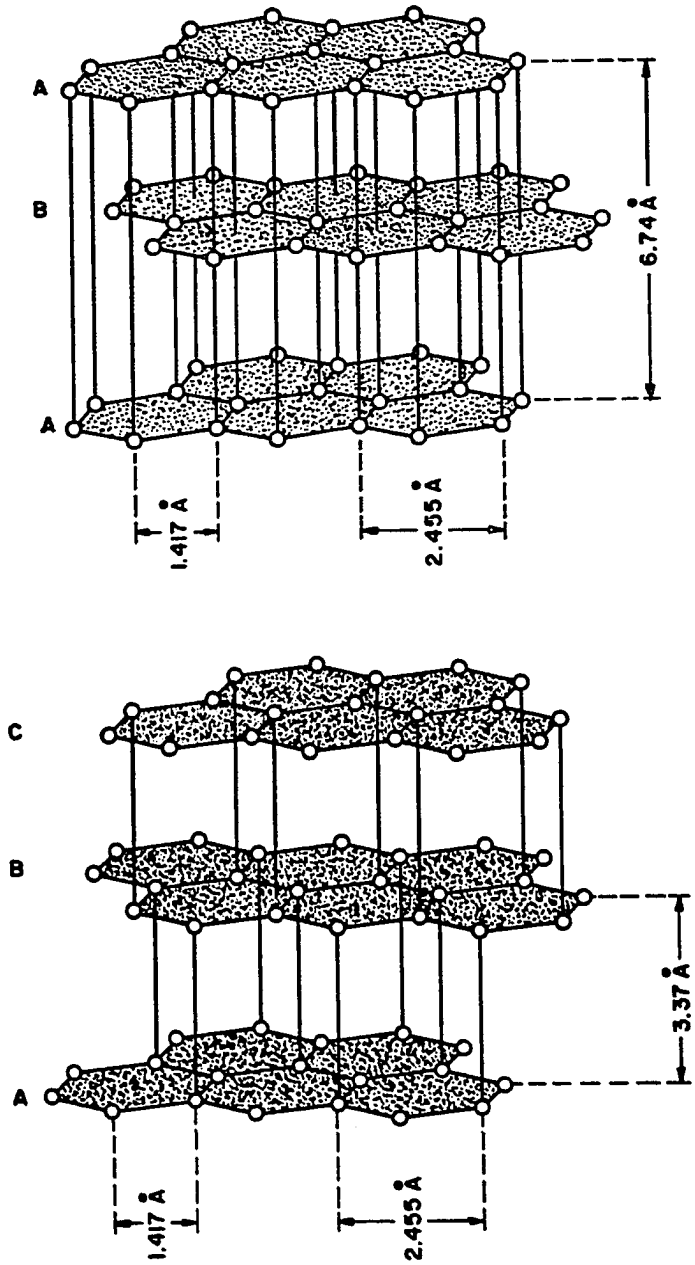

Fig. 3.2. Crystal structures of graphite.
From Shobert (1964).

The optical properties of graphite depend on the direction of the E-field with respect to its optical c-axis, $E \perp C$ and $E \parallel C$ leading to $\varepsilon_{\perp}$ and $\varepsilon_{\parallel}$ respectively. Because samples can easily be prepared by cleavage of the crystal in the basal plane, many optical constants for the $E \perp C$ direction are available in the literature. Fewer measurements have been done for $E \parallel C$ since the sample preparation is considerably more difficult in this case. $E \perp C$ and $E \parallel C$ optical constants of graphite will be reviewed in turn.

Survey of Optical Constants of Graphite

Many workers measured reflectance on natural graphite, pyrolytic graphite or annealed pyrolytic graphite. They analyzed their data by the Kramers-Kronig method (Taft and Philipp, 1965; Philipp, 1977), by fitting (Greenaway et al., 1969; Klucker, Skibowski, and Steinman, 1974) or by the use of Fresnel's equations (Carter et al., 1965).

Zeppenfeld (1967) was the first to use the electron energy loss method for deriving optical constants of graphite. This method consists of determining the properties of bulk materials by measuring the transmission of electron beams through thin films. ε_1 and ε_2 are obtained by the Kramers-Kronig analysis of the energy loss function $f(\omega)$ which is related to the dielectric function by (Daniels et al., 1970):

$$f(\omega) = - \mathrm{Im}\ (1/\varepsilon) \quad .$$

The survey of optical constants is summarized in Table 3.2.

Comparison of results for $E \perp C$ is seen in Fig. 3.3a which shows ε_2 in a spectral range which contains a strong peak. Good agreement exists in the shape of the curve, but the discrepancy in the magnitude of the peak is obvious.

For $E \parallel C$, Fig. 3.3b shows complete disagreement between the results of the reflectance techniques and those of the electron energy-loss method. Because of the severity of the discrepancy, Venghaus (1975) repeated the electron energy-loss measurements on graphite. His results were in agreement with the measurements done with the same technique by other workers, but still in disagreement with reflectance method results. Wessjohan (Venghaus, 1975) computed reflectance using Venghaus (1975) and Klucker et al. (1974) ε data; Venghaus's results compared favorably with experiments, but those from Klucker et al. failed to do so. Although Klucker (1971), who noticed the discrepancy between his experimental results and calculations, assigned this failure to scattered light, Venghaus concluded that the electron energy-loss method gives better results.

In IR ($\lambda \sim 2.5$ μm to 100 μm), Venghaus measured the reflectance on graphite in the E//C direction and analyzed the data by the Kramers-Kronig method.

Table 3.2. Survey of optical properties of graphite.

Reference	Range (μm)	Technique	Polarization	Comments
Carter et al. (1965)	0.11 - 0.30	Reflectance	E ⊥ C	Agreement with Taft and Philipp
Ergun (1967)	0.55	Reflectance	E ⊥ C, E // C	High values of n
Foster & Howarth (1968)	1 - 9.2	Reflectance	E // C	High IR results
Greenaway et al. (1969)	0.25 - 0.62	Multi-angle reflectance	E ⊥ C, E // C	Compares well with this work
Klucker et al. (1974)	0.03 - 0.41	Multi-angle reflectance	E ⊥ C, E // C	Very low values of ε_2
Lenham & Treherne (1966)	0.4 - 19	Reflectance	E ⊥ C, E // C	
Philipp (1977)	1 - 1239	Reflectance	E ⊥ C	Sato reflectance results used
Sato (1968)	41 - 206	Reflectance	E ⊥ C	Did not take free electron behavior into consideration in his analysis
Venghaus (1975)	0.03 - 1.2	Energy-loss	E ⊥ C, E // C	Agreement with Zeppenfeld
Venghaus (1977)	2.5 - 83	Reflectance	E // C	Published results

Table 3.2--Continued

Reference	Range (μm)	Technique	Polarization	Comments
Taft & Philipp (1965)	0.05 - 41	Reflectance	E ⊥ C	Commonly accepted results
Zeppenfeld (1967)	0.03 - 1.2	Energy-loss	E ⊥ C, E // C	First to use energy-loss techniques on graphite

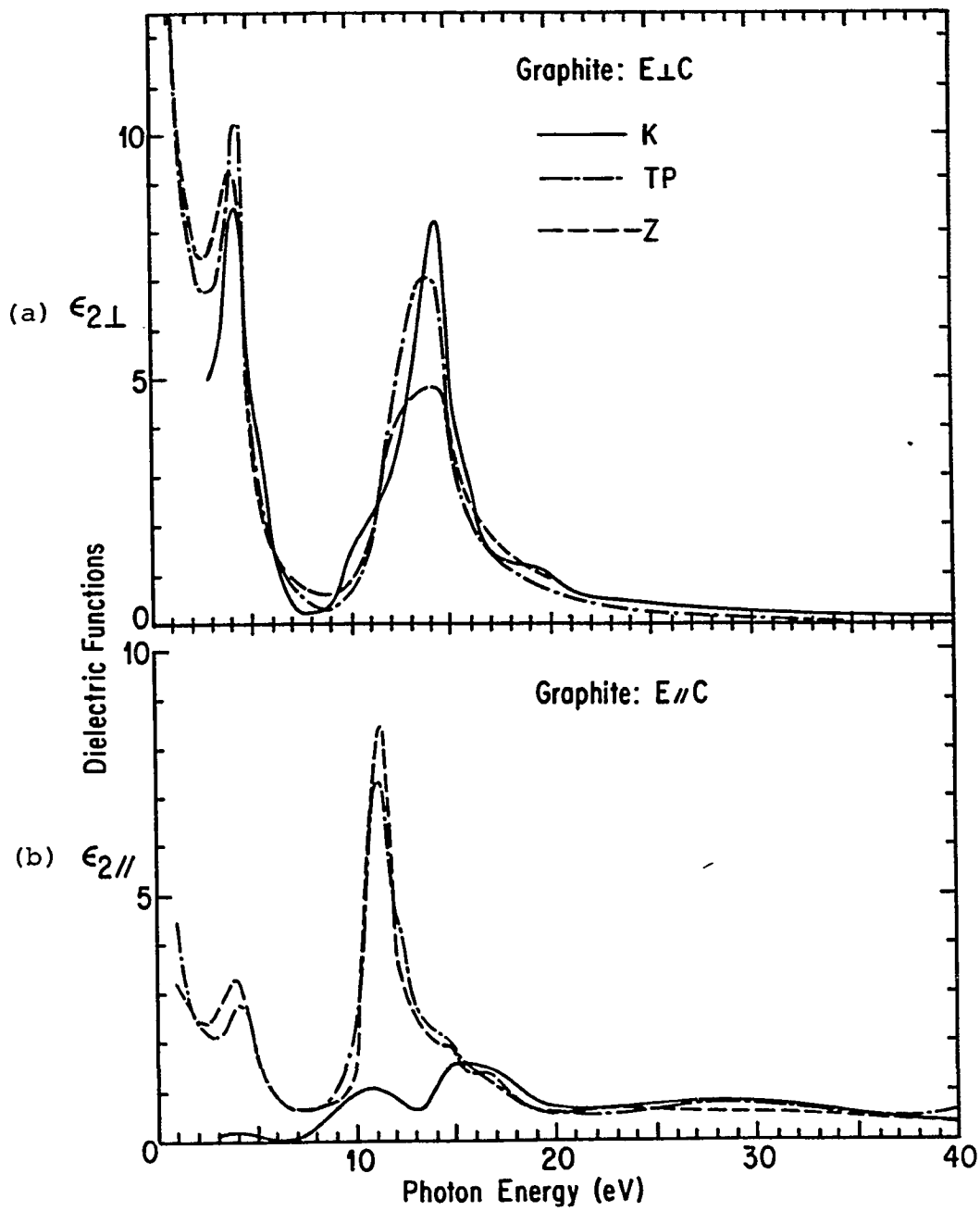

Fig. 3.3. Imaginary part of the dielectric function for the E ⊥ C (a) and E // C (b) polarizations of graphite.

As computed by Klucker et al. (1974), Taft and Philipps (1965), and Zeppenfeld (1967).

This Study's Investigation on Graphite

In order to have a coherent set of optical constants in a broad spectral range for the E $\perp$ C direction of graphite, and also to investigate the discrepancy of the ε_2 peak at $\lambda \sim 0.088$ μm, Philipp's (1977) extended reflectance data (see Fig. 3.4) have been analyzed by the Kramers-Kronig method. Philipp obtained his extended reflectance data by combining previously published results (Taft and Philipp, 1965), measurements between $\lambda \sim 12.4$ μm and 41 μm, and Sato's (1968) data.

It is known that the Kramers-Kronig analysis results depend strongly on the extrapolation at low wavelengths (Wooten, 1972). To satisfy the requirements of the extrapolation, which is explained in Chapter 2, some guide values of n and k found from an independent experiment are needed. Huffman (1979), in work done at the University of Wisconsin monochromatic radiation facility, measured the transmission of a 0.27 μm thick cleaved graphite sample from $\lambda \sim 1.25$ μm to 0.15 μm. The values of n and k found from this experiment have been used as tests for the choice of the parameter s and the wavelength λ. These values are $s = 2$, $\lambda_f \sim 0.0258$ μm. Taft and Philipp used the results of the transmission of a 400Å thick sample from $\lambda \sim 0.113$ μm to 0.177 μm as guiding values in their calculations. Results of our calculations are shown in Figs. 3.5, 3.6, and 3.7 and in Appendix A.

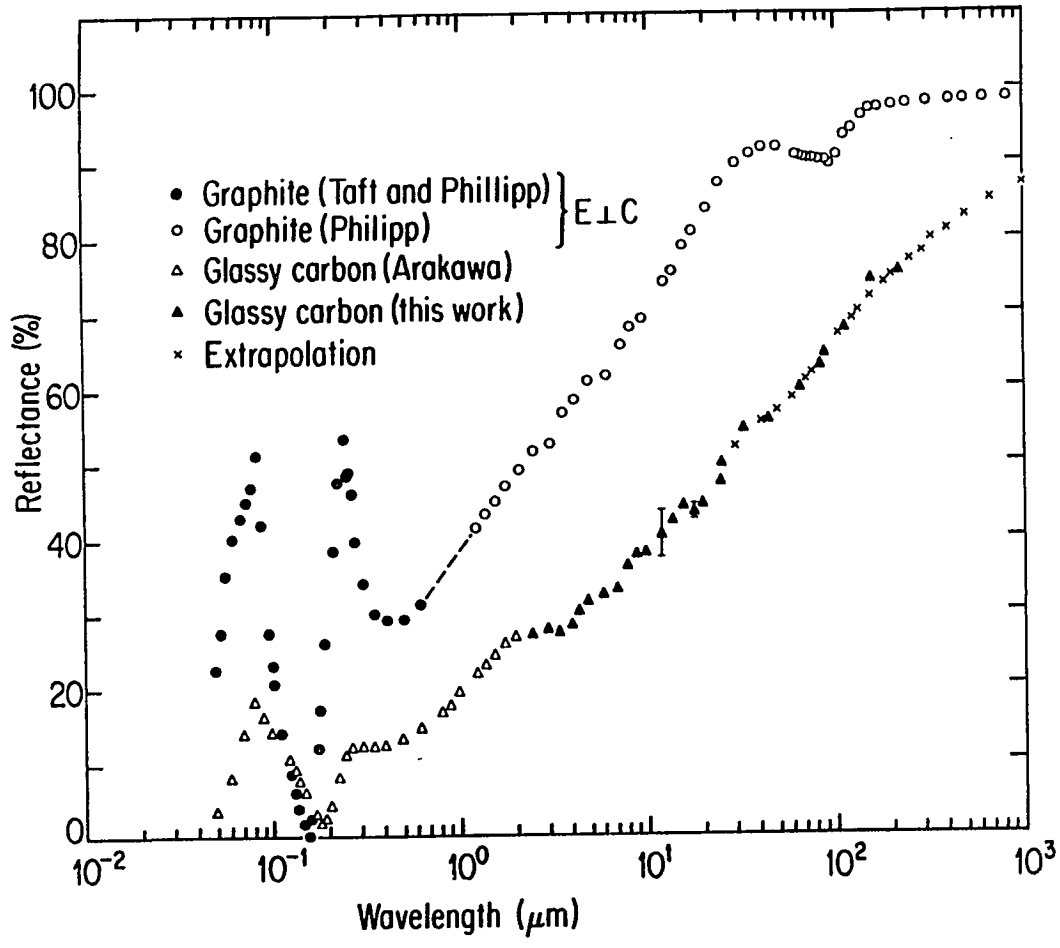

Fig. 3.4. Reflectance of graphite and glassy carbon.

Graphite (Taft and Philipp, 1965; Philipp, 1977), glassy carbon (Williams and Arakawa, 1972 and this work).

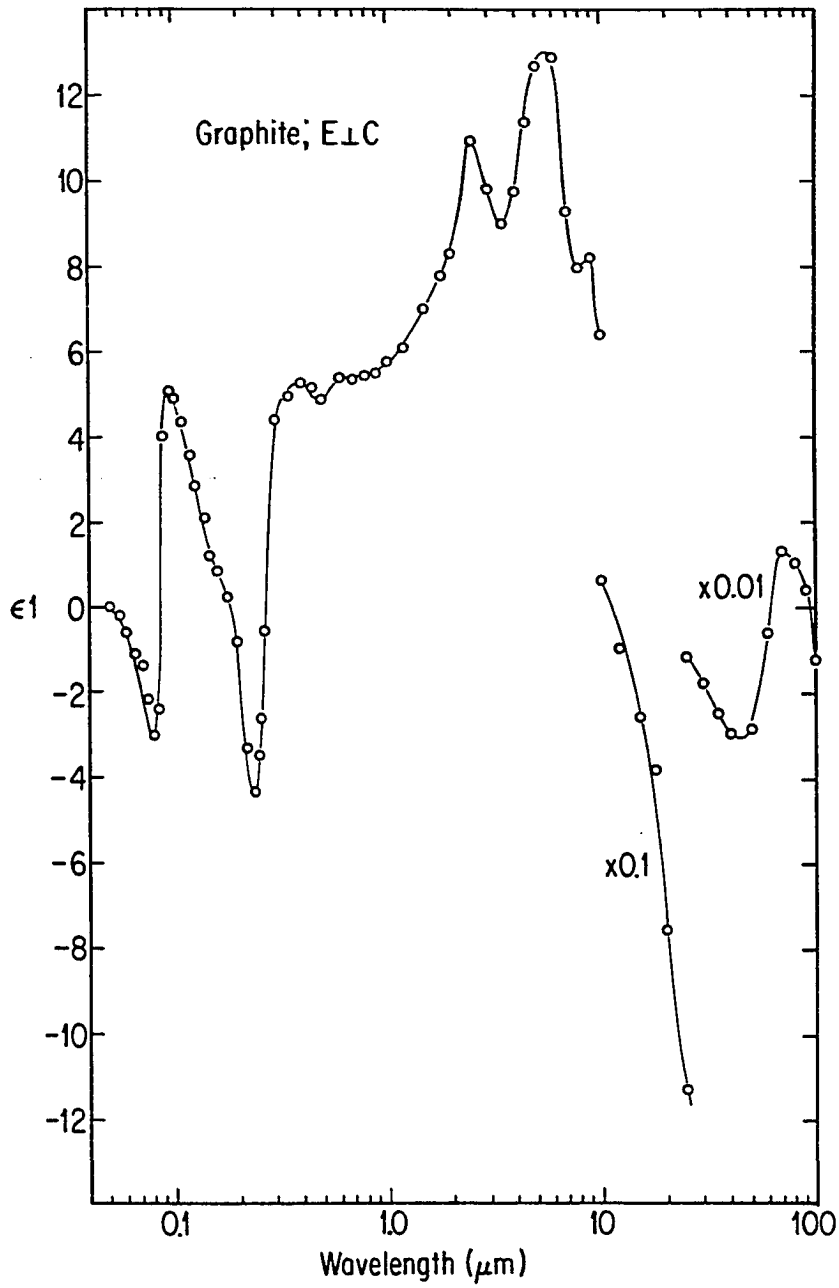

Fig. 3.5. Real part of the E ⊥ C polarization of graphite as computed by the Kramers-Kronig method.

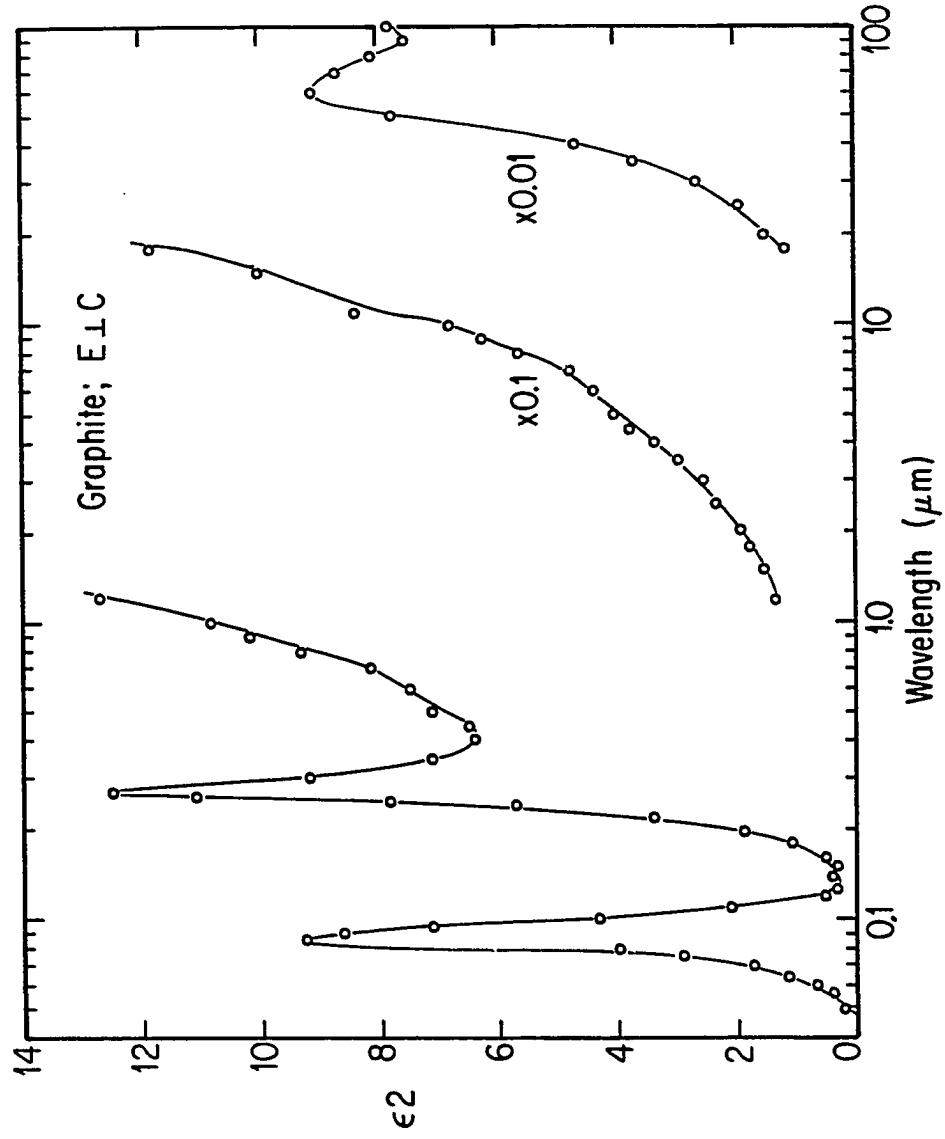

Fig. 3.6. Imaginary part of the E ⊥ C polarization of graphite as computed by the Kramers-Kronig method.

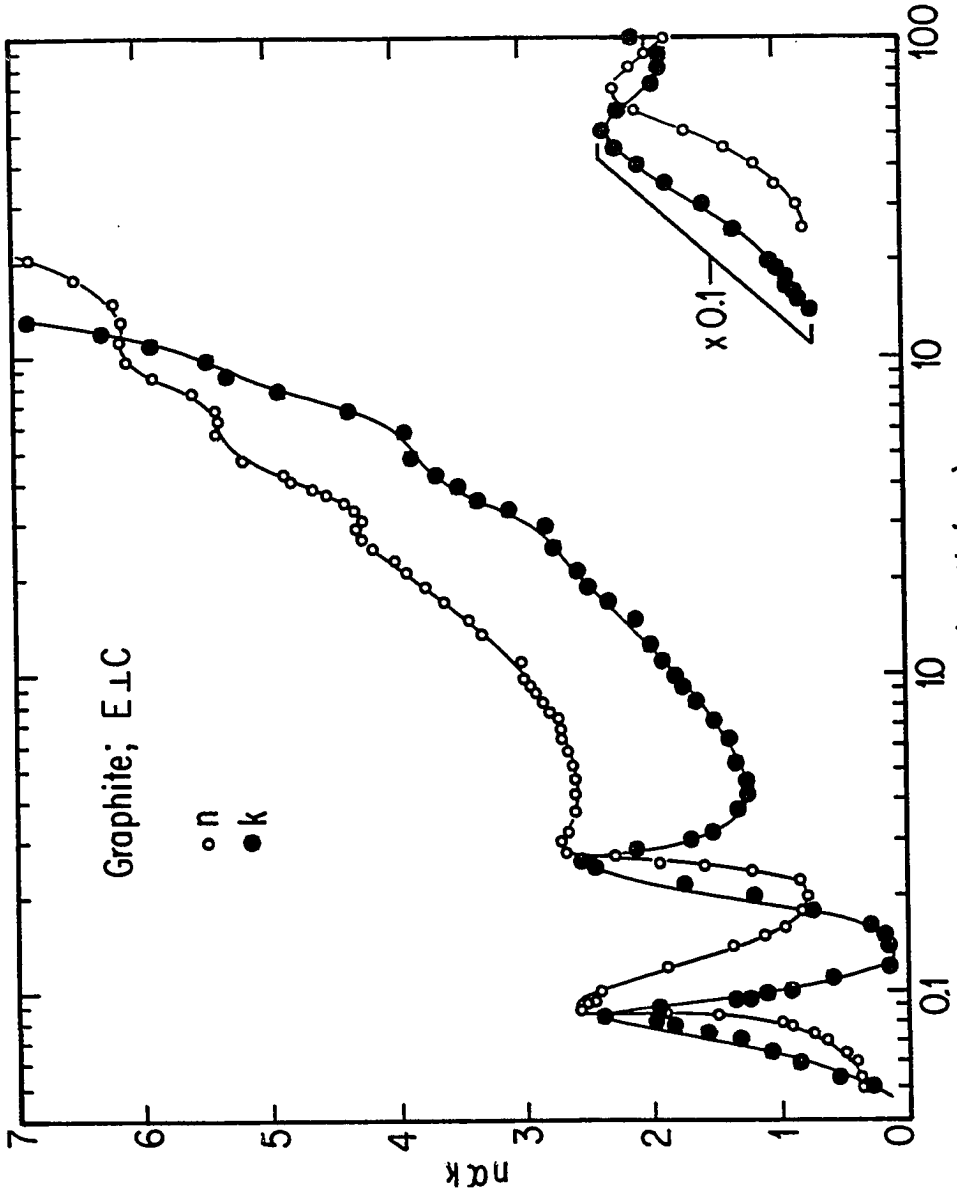

Fig. 3.7. Optical constants n and k for the E ⊥ C polarization of graphite computed by the Kramers-Kronig method.

The reflectance data fit result is shown in Fig. 3.8. A discussion of the discrepancy observed between the data and the fit from λ = 0.3 to 15 μm is given in the "Discussion of Results" section of this chapter. The oscillator parameters used are presented in Table 3.3.

Representative values of ε_1 and ε_2 for the E // C direction of graphite derived from the reflectance and the electron energy-loss measurements have been converted to n and k and plotted (Fig. 3.9). Venghaus's results below $\lambda \sim 2.5$ m were obtained privately. Venghaus (1977) argued that reflectance measurements are not seriously affected by the roughness of the reflectance surface in the IR wavelength range; n and k obtained by optical methods are thus reliable from 2.5 μm to 100 μm. In the short wavelength range ($\lambda \sim 0.03$ to about 0.22 μm), the increasing dependence on the reflectance on the state of the surface as the wavelength decreases makes the results of the optical method less reliable than those obtained with the electron energy-loss technique. Since above $\lambda \sim 0.25$ μm, the Cerenkov radiation gives the dominant contribution to the electron energy-loss for E // C (Tossati and Bassani, 1970), the electron energy-loss results have been disregarded from $\lambda \sim$ 0.25 μm to 2.5 μm. From 0.15 μm to 0.25 μm, geometrical considerations have been used. The slope of the electron energy-loss n curve at short $\lambda \sim 0.15$ μm is the same as the slope of the reflectance n curve from $\lambda \sim 0.21$ μm to 0.25 μm.

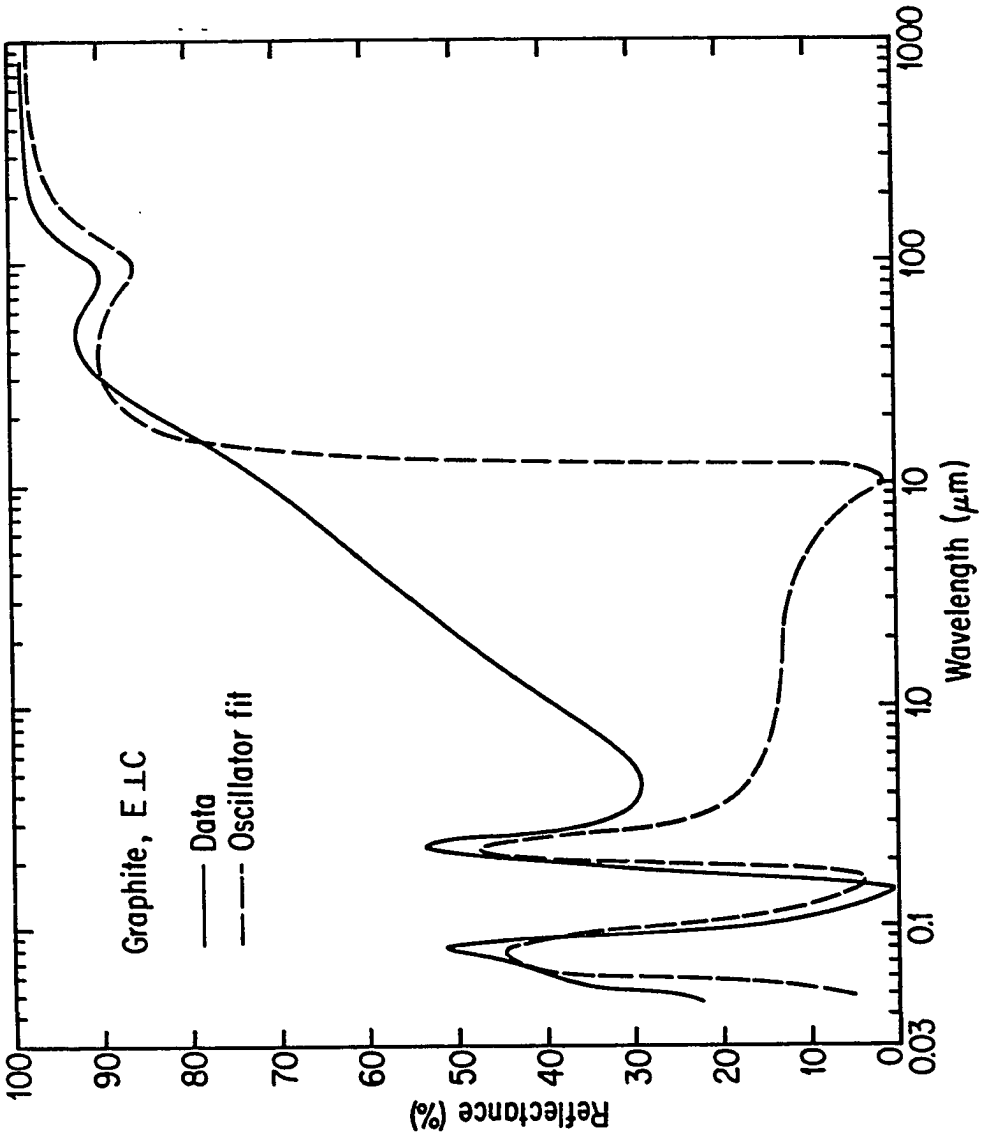

Fig. 3.8. Oscillator fit of the reflectance of graphite (E ⊥ C polarization).

Table 3.3. Oscillator parameters for the fit of the reflectance curve for the E $\perp$ C direction of graphite.

	Parameter	Value (cm^{-1})
Oscillator 1	ω_{P1}	1200
	ω_1	0.00
	γ_1	15.00
Oscillator 2	ω_{P2}	1300
	ω_2	120
	γ_2	120
Oscillator 3	ω_{P3}	6×10^3
	ω_3	4×10^3
	γ_3	7.5×10^3
Oscillator 4	ω_{P4}	110×10^3
	ω_4	98×10^3
	γ_4	25×10^3

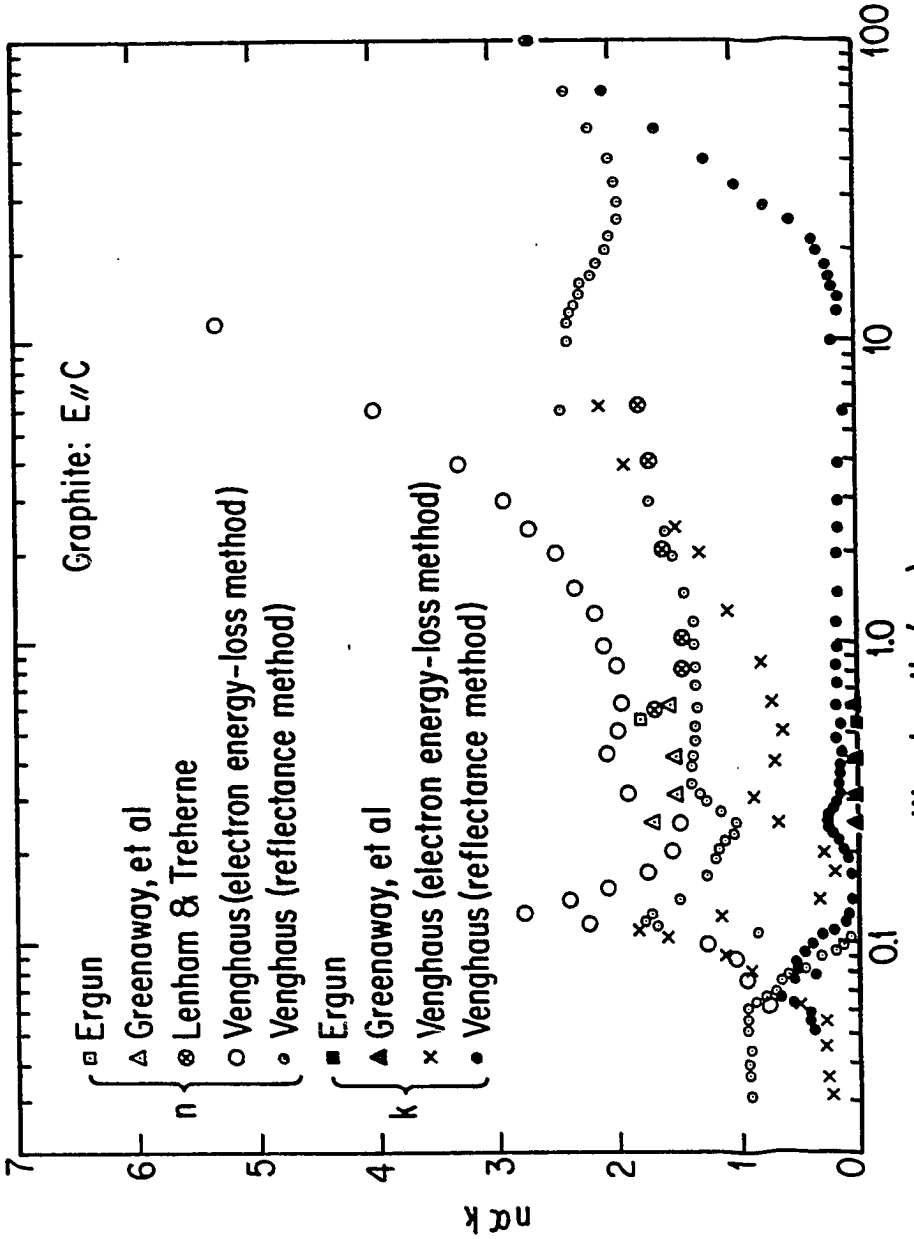

Fig. 3.9. Optical constants n and k of the E // C polarization of graphite.

Based on that consideration, a connecting curve has been drawn between the two n curves from $\lambda \sim 0.15$ μm to 0.21 μm. From this combination of optical method results and electron energy-loss measurements, a set of n and k data for E // C has been put together from $\lambda \sim 0.025$ μm to 100 μm. (See Figs. 3.10 and 3.11 and Appendix A.)

For the E // C direction of graphite, the reflectance computed from n and k extracted from the literature has been fitted using a Drude-Lorentz oscillator model; the result is shown in Fig. 3.12. The oscillator parameters used are presented in Table 3.4.

Glassy Carbon

Glassy carbon, also known as vitreous carbon, is produced by the slow pyrolysis of polymers such as cellusen and aromatic resins. It looks like black glass, has a low density (1.4 - 1.5 g/cm^3) and also a low porosity and permeability to water. It has about the same hardness as glass; it withstands high temperature in absence of oxygen. X-ray studies have shown that glassy carbon has randomly oriented crystals which are not very much altered by heat treatment. At 3273°K, glassy carbon crystallite size is 6 mm; they are smaller at lower temperatures (Halpin and Jenkins, 1969).

Taft and Philipp (1965) published near normal incidence reflectance data of glassy carbon up to 26 eV. Williams and Arakawa (1972) published plots of n and k

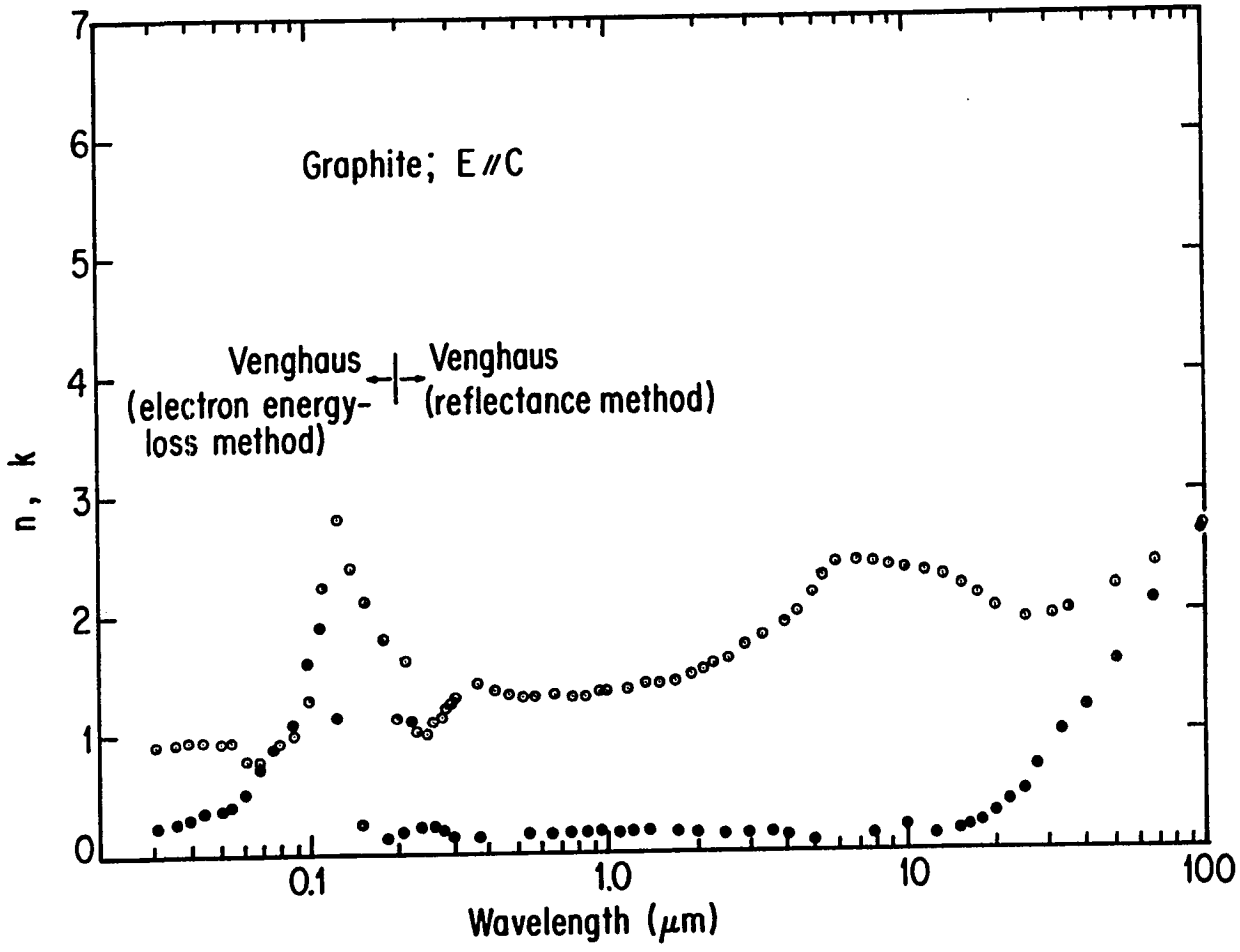

Fig. 3.10. Adjusted optical constants n and k of the E // C polarization of graphite.

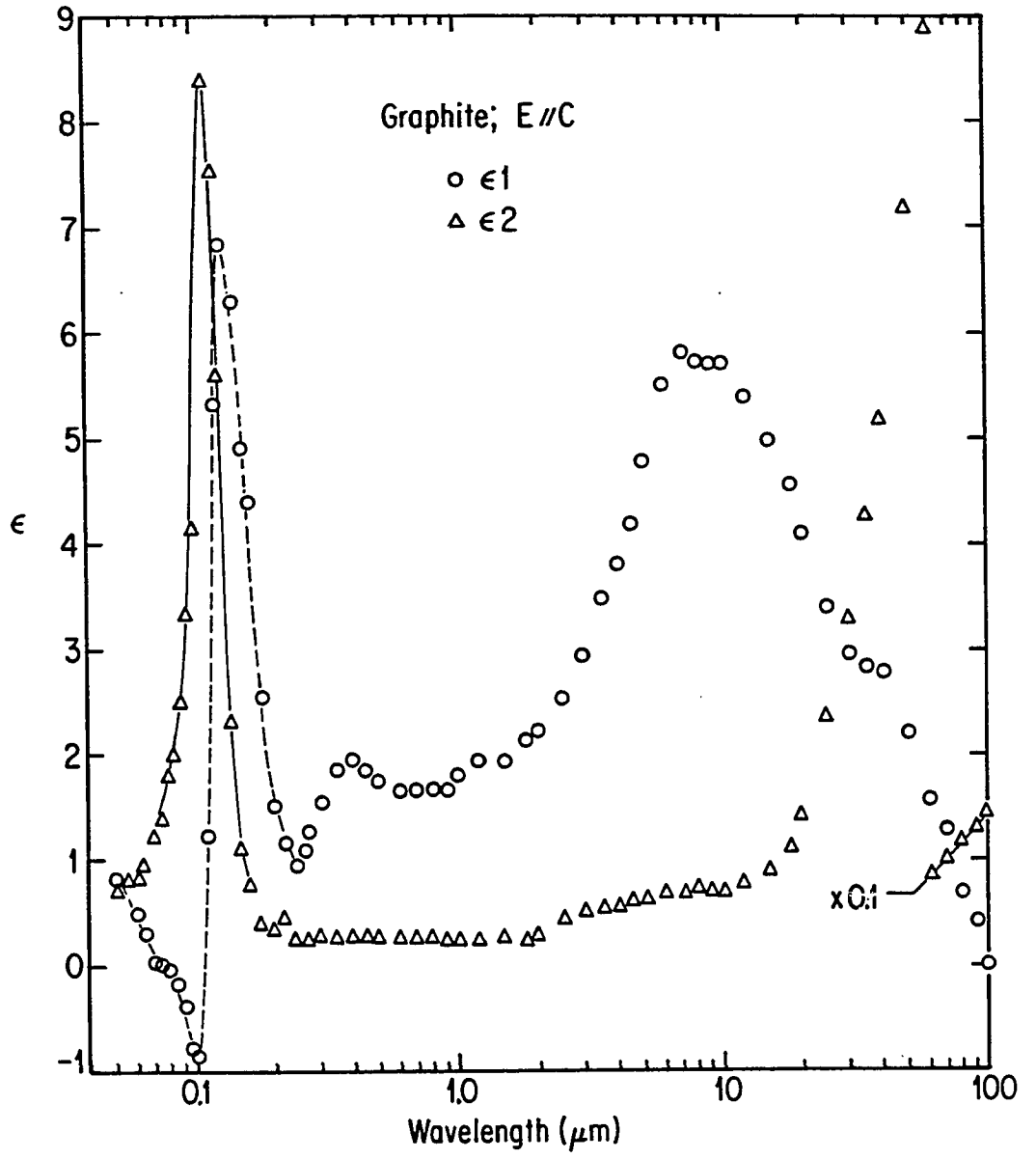

Fig. 3.11. Real and imaginary parts of the dielectric function of the E // C polarization of graphite.

As computed with the use of the adjusted optical constants of Fig. 3.10.

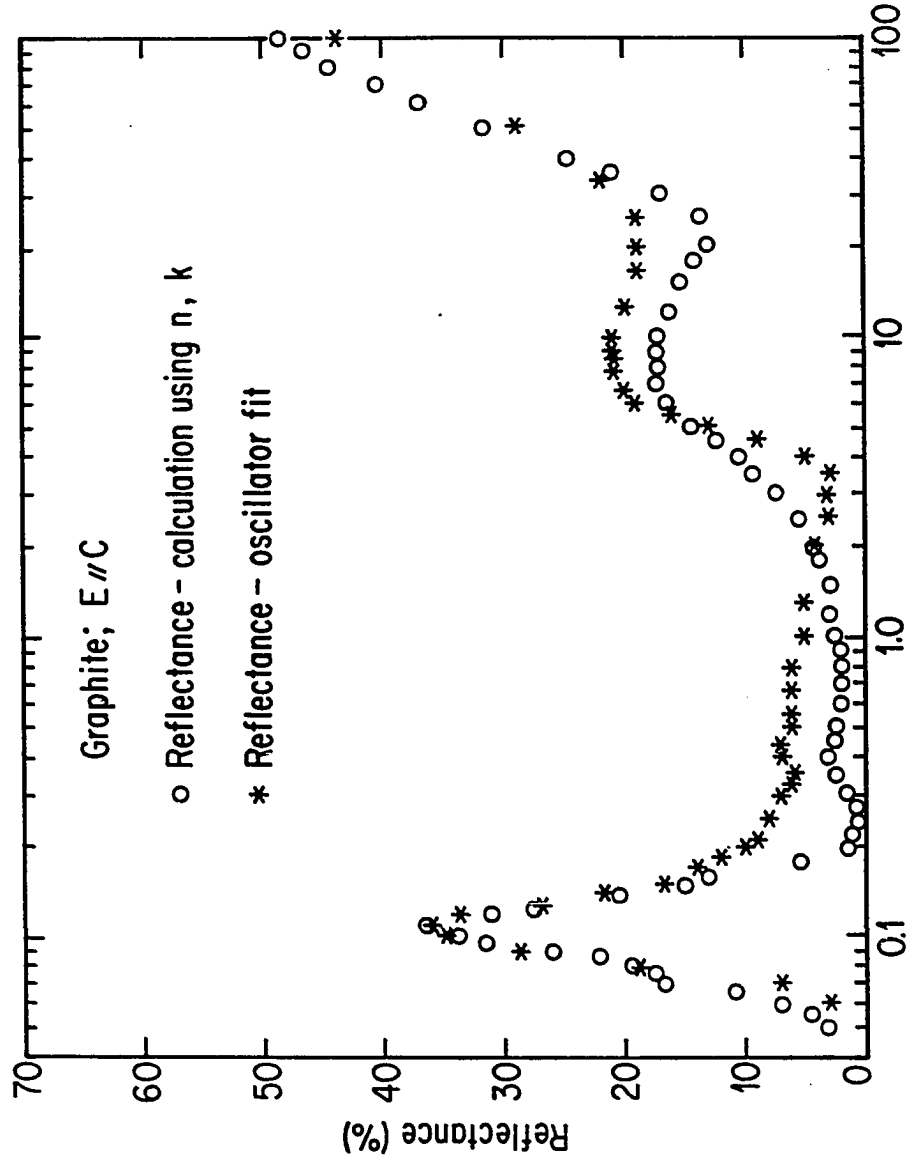

Fig. 3.12. Reflectance of the E // C polarization of graphite.

Table 3.4. Oscillator parameters for the fit of the reflectance curve for the E // C direction of graphite.

	Parameter	Value (cm^{-1})
Oscillator 1	ω_{P1}	8500
	ω_1	0.00
	γ_1	900
Oscillator 2	ω_{P2}	2950
	ω_2	1500
	γ_2	1500
Oscillator 3	ω_{P3}	5,000
	ω_3	25,000
	γ_3	3,000
Oscillator 4	ω_{P4}	95,000
	ω_4	75,000
	γ_4	25,000

of glassy carbon from 0 to 82 eV, but it is practically impossible to obtain any detailed information below about 0.2 eV. It was therefore necessary to complete the available information.

In this study, optical constants based on the analysis of reflectance measurements extending to 225 μm and a Drude fit to reflectance extending to 1000 μm have been derived. The instruments used in the experiment, along with the near normal reflectance measurements will be presented; then the data analysis will be discussed.

Instrumentation and Measurements

Spectrophotometers to which suitable reflectometers (Steyer, 1974) have been attached were used for the measurements. A Cary 14 was used in the visible and in the near IR, a Perkin Elmer 398 in the IR, and a Beckman IR 11 for the far IR (see Table 3.5).

The Cary 14 and the Perkin Elmer 398 were used in a double beam mode, and the Beckman 11 in a single beam mode. The Beckman 11 was modified to use a liquid He cooled, doped germanium bolometer as a detector. The signal obtained was amplified by a PAR model 28 lock-in amplifier and then sent to a digital voltmeter or chart recorder (Rathmann, 1981).

The reflectometers were designed to give a near normal incidence reflectance. The one used on the Cary 14

Table 3.5. Spectral region and instrument.

From Rathmann (1981).

Region	Wavelength (Frequency)	Instrument	Spectral Resolution
Far IR	250 μm - 20 μm (40 - 500 cm^{-1})	Beckman IR 11	∿ 5 cm
Mid IR	25 μm - 2.5 μm (400 - 4000 cm^{-1})	Perkin Elmer 398	∿ 5 cm
Near IR to Visible	2 μm - 0.33 μm (5000 - 3.3 x 10^4 cm^{-1})	Cary 14	∿ 10 Å

and the Perkin Elmer 398 is built by Barnes Engineering Company; the far IR one was designed and built in our lab.

An aluminized glass reference was used. Good alignment was always checked before any measurement; the aluminum standard or the sample was positioned and the mirrors of the reflectometer rotated until a maximum signal was obtained.

The measurement procedure was as follows:

1. Run the 100% reflectance line, say R_{100}, with the aluminum standard in place.
2. Run the zero reflectance line, say R_0, without any sample.
3. Run the reflectance of a well-polished sample, say R_S.

From the spectrum obtained, it is easy to find:

$$R'(\lambda) = \frac{R_S - R_0}{R_{100} - R_0} ,$$

where $R'(\lambda)$ is a relative reflectance; this data can be used in the Kramers-Kronig analysis computer program where it is converted into an absolute reflectance.

Reflectance from $\lambda \sim 0.35$ μm up to 220 μm has been measured and good agreement obtained with Arakawa's published results in the 0.3 μm to 2.5 μm wavelength range which the experiments have in common. It was thus not

necessary to pursue measurements toward wavelengths shorter than 0.35 μm.

Data Analysis and Results

For use in the Kramers-Kronig analysis, reflectance was extended toward long wavelengths by curve fitting. Free electron behavior was assumed for glassy carbon at larger wavelengths than the last experimental point, and the Drude model used in the fitting. The parameters used were: $\omega_P = 2000\ cm^{-1}$; $\omega_j(1) = 0$, and $\gamma = 900\ cm^{-1}$. Reflectance data going from $\lambda \sim 0.02$ μm to about 10^6 μm were constructed by combining Williams and Arakawa's (1972) results, experimental results of this study, and extrapolated results, for use in the Kramers-Kronig analysis (see Fig. 3.4). The results of the analysis are presented in Figs. 3.13 to 3.15 and in Appendix A.

We then proceed to use the Drude-Lorentz model and fit the reflectance data obtained for the Kramers-Kronig study; the result is shown in Fig. 3.16, and the parameters used are presented in Table 3.6.

Discussion of Results

The reflectance data for graphite in the E ⊥ C orientation and that of glassy carbon have been analyzed by the Kramers-Kronig method and by fitting a Drude-Lorentz model to the reflectance curves. The reflectance data for graphite in the E // C orientation has only been fitted

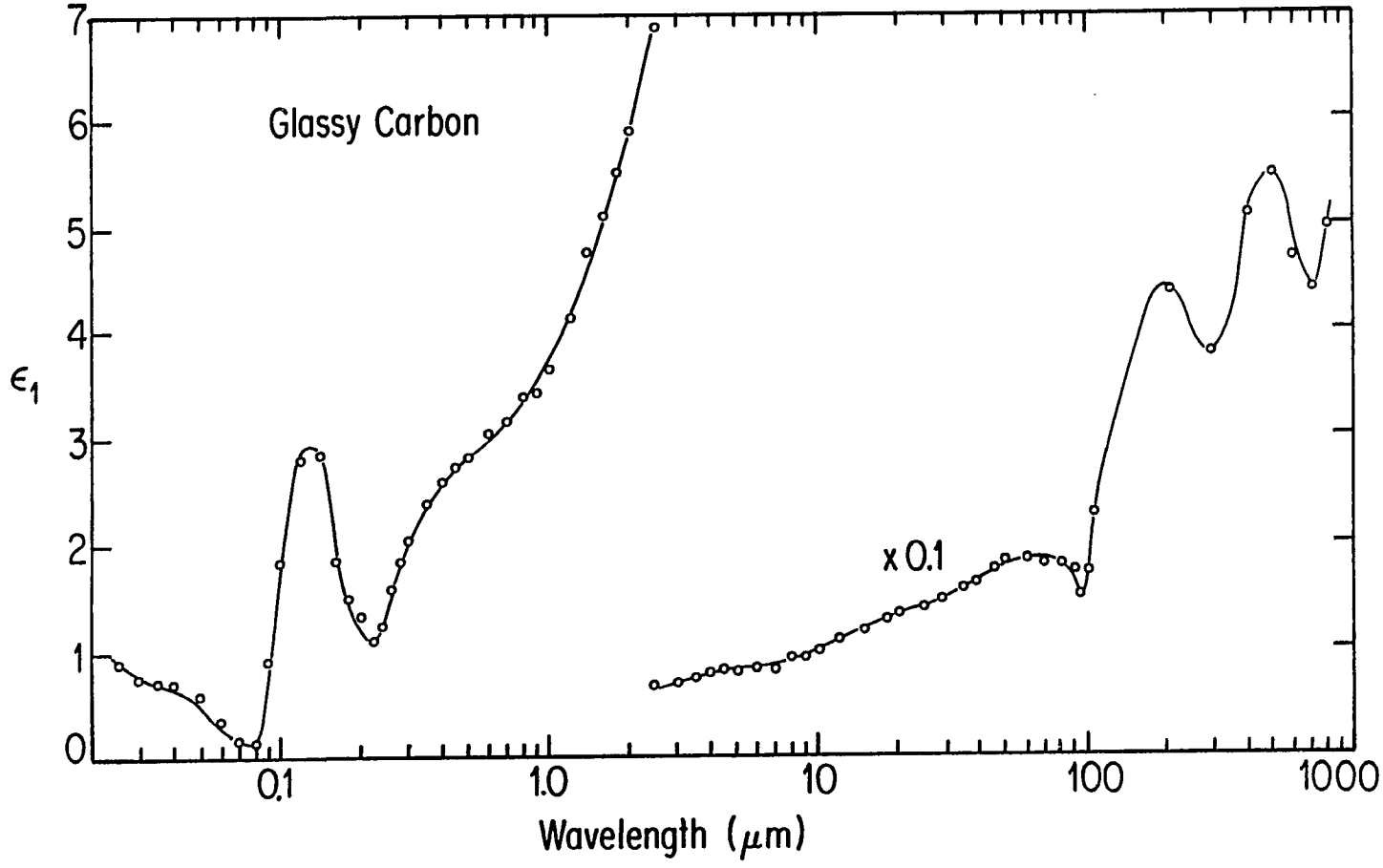

Fig. 3.13. Real part of the dielectric function of glassy carbon, as computed by the Kramers-Kronig method.

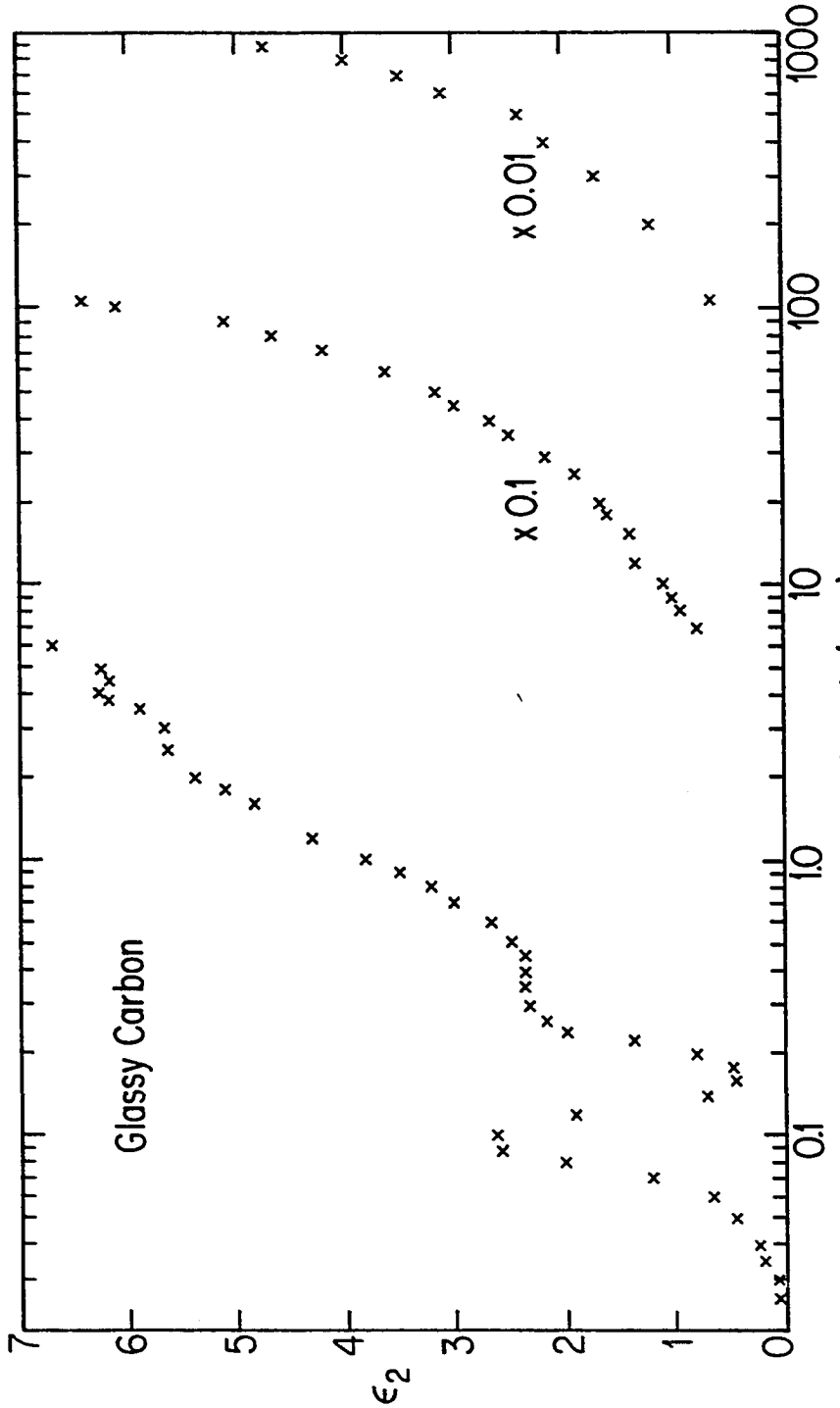

Fig. 3.14. Imaginary part of the dielectric function of glassy carbon, as computed by the Kramers-Kronig method.

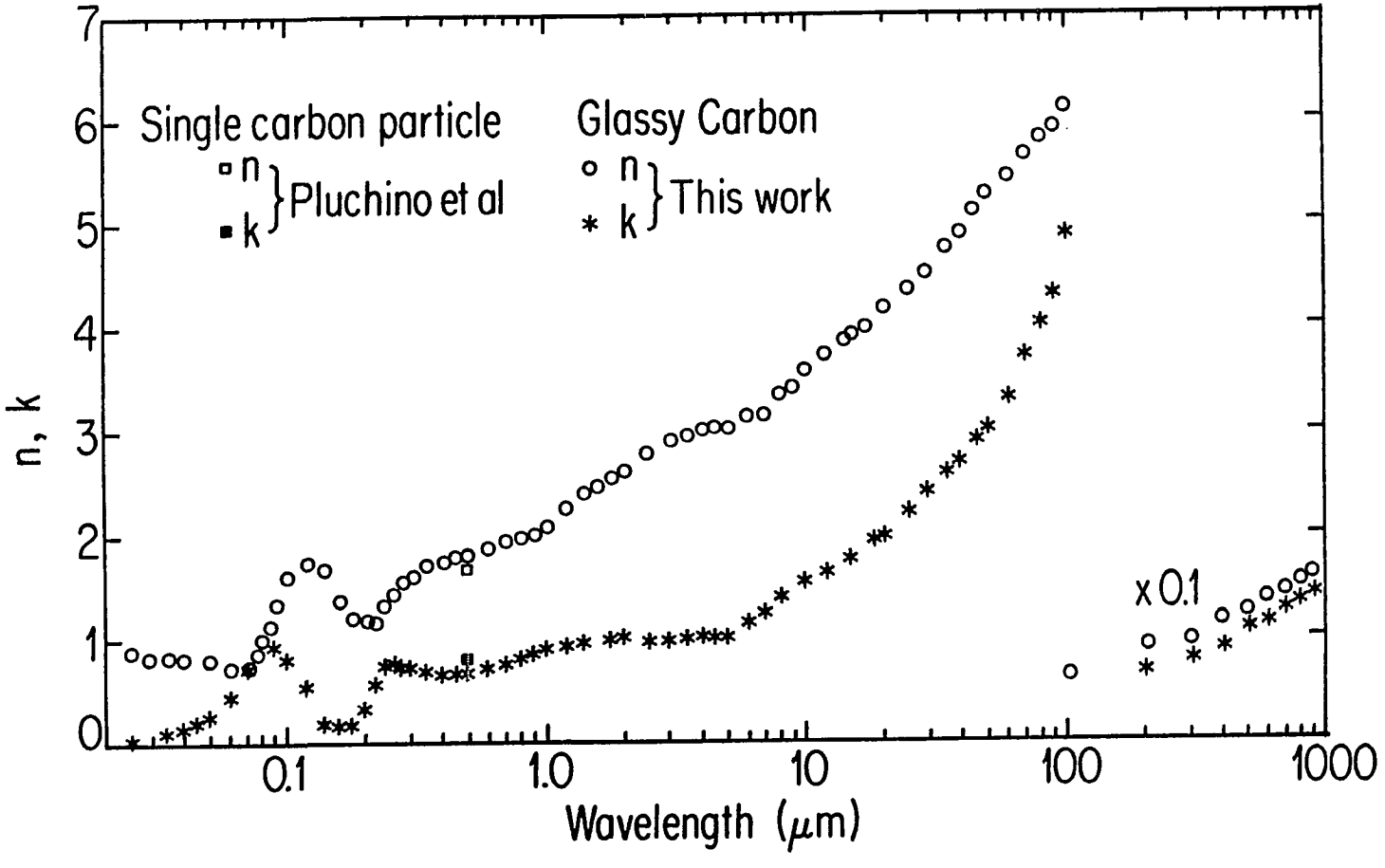

Fig. 3.15. Optical constants n and k of glassy carbon as computed by the Kramers-Kronig method and comparison to Pluchino et al. (1980) results.

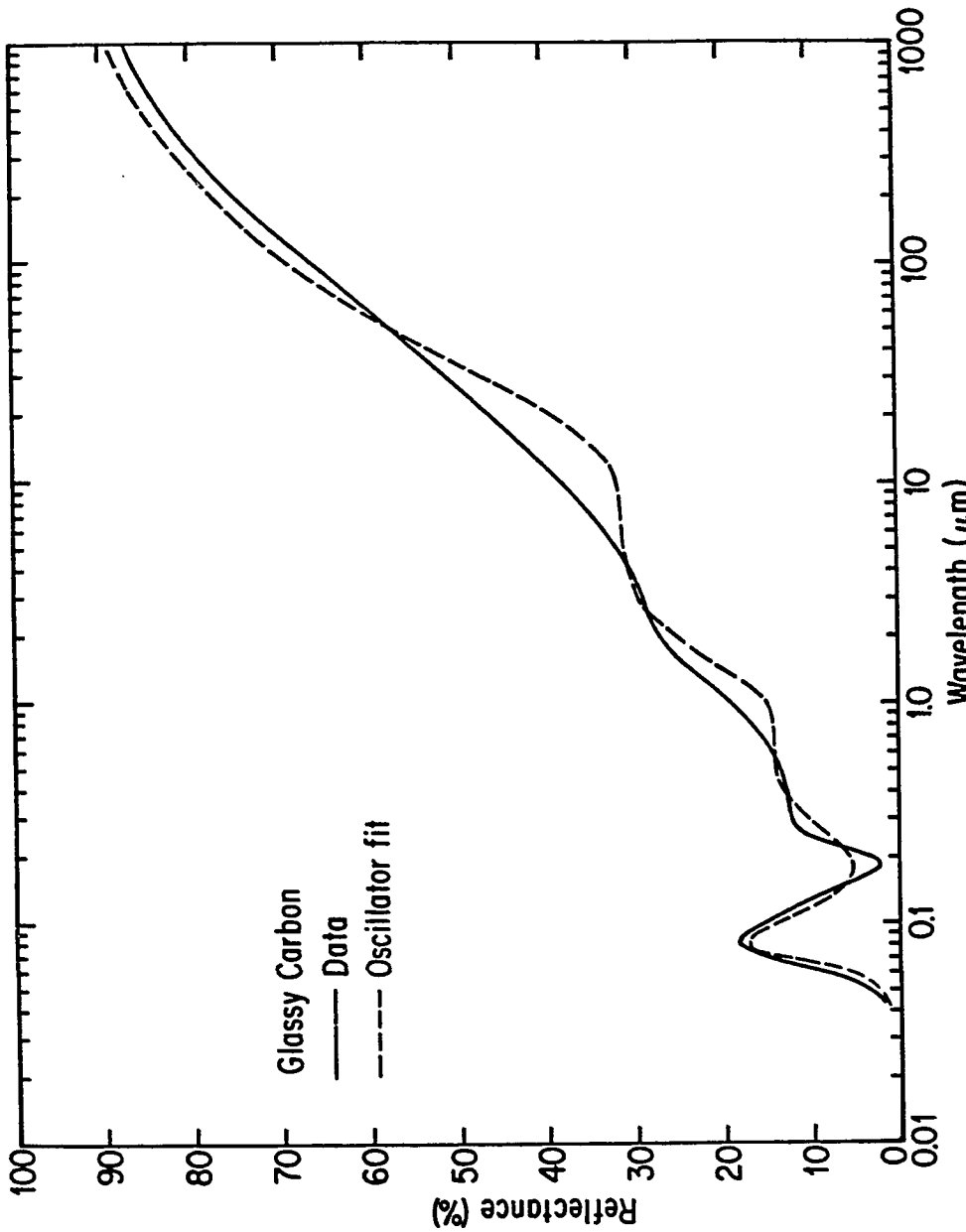

Fig. 3.16. Oscillator fit of the reflectance of glassy carbon.

Table 3.6. Oscillator parameters for the fit of the reflectance curve of glassy carbon.

	Parameter	Value (cm^{-1})
Oscillator 1	ω_{P1}	4000
	ω_1	0.00
	γ_1	1000
Oscillator 2	ω_{P2}	14.5×10^3
	ω_2	5×10^3
	γ_2	9×10^3
Oscillator 3	ω_{P3}	50×10^3
	ω_3	30×10^3
	γ_3	43×10^3
Oscillator 4	ω_{P4}	120×10^3
	ω_4	110×10^3
	γ_4	60×10^3

because the spectral range of the data was not large enough to allow the use of the Kramers-Kronig method.

In all the fits, the oscillator strength parameters (ω_{pj}^2) have been checked against the sum rule (see Kittel, 1976, p. 351 and Wooten, 1972, p. 72):

$$\int_0^\infty \omega\epsilon_2(\omega)\, d\omega = \sum_j \omega_{pj}^2 = \tfrac{1}{2}\pi\omega_p^2 \quad . \tag{41}$$

The plasma frequency ω_p is given by (see Kittel, 1976, p. 289):

$$\omega_p = \frac{4\pi ne^2}{m} \quad , \tag{42}$$

where n is the density of electrons, e and m the charge and the mass of an electron in c.g.s. units. With the assumption that all the four valence electrons of carbon determine ω_p, one obtains:

$$\tfrac{1}{2}\pi\ \omega_p^2 \simeq 20.3 \times 10^{32}\ \text{sec}^{-2} \quad .$$

The value of $\sum_j \omega_{pj}^2$ for each case is given in Table 3.7. In each of the three cases

$$\sum_j \omega_{pj}^2 < \tfrac{1}{2}\pi\ \omega_p^2 \quad .$$

Table 3.7. Values of $\sum_j \omega_{Pj}^2$.

Material	$\sum_j \omega_{Pj}^2$ (sec^{-2})
Graphite: E ⊥ C	$\sim 4.4 \times 10^{32}$
Graphite: E // C	$\sim 3.3 \times 10^{32}$
Glassy carbon	$\sim 6.2 \times 10^{32}$

This result is expected, since the maximum possible value for n has been chosen for substitution in Eq. (42). Some valence electrons might be sufficiently bound that the sum rule (Eq. 41) is not satisfied over the frequency range of the experiment.

The discrepancy between the experimental and fitted curves observed between λ = 0.3 and 15 μm on Fig. 3.8 is due to interband transitions which come into play with increasing energy. These transitions gradually increase the reflectance without showing sharp peaks. The Lorentz model used for the fit cannot account well for this phenomenon. The fit of the peak at $\lambda \sim 45$ μm resulted in the sharp drop in the calculated reflectance.

The band structure of graphite as calculated by Mallett (1981) shows narrow band gaps at $\lambda \simeq 0.08$ and 0.25 μm, which account for direct interband transitions, responsible for the sharp peaks observed at those wavelengths. These peaks were easily fitted.

Examination of Figs. 3.12 and 3.16 shows that to some extent, the reflectance of the E // C polarization for graphite and that of glassy carbon have the same behavior as the reflectance of the E $\perp$ C orientation for graphite. This behavior makes the fit difficult between λ = 0.3 and 15 μm, but the difference between the experimental reflectance and the fit is unimportant because of the low reflectance of the materials considered.

Results obtained by the two methods of analysis for glassy carbon are compared in Table 3.8 for several wavelengths.

Comparing this Kramers-Kronig analysis with published data, one finds that for the E ⊥ C orientation of graphite, the optical constants derived agree well with those of Taft and Philipp (1965) (see Table 3.9) and Greenaway et al. (1969). At the peak around $\lambda \sim 0.088$ μm, our value of 9.3 for ε_2 is higher than that of Taft and Philipp's (1965) value of ~ 7.0. The difference is due to the values of the parameters used in the short wavelength extrapolations for the Kramers-Kronig analysis (see p. 34).

The optical constants obtained for the E ⊥ C orientation of graphite are to our knowledge the only consistent ones available at this writing.

The glassy carbon optical constants agree well with Williams and Arakawa's (1972) results and extend them beyond $\lambda \sim 10$ μm. Differences exist between our results and those published for varouis amporphous carbons as one can readily see in Fig. 3.1. One exception is the result of Pluchino et al. (1980) (see Fig. 3.15). The good agreement in this case is worth pointing out, even though the comparison is possible for one wavelength only. Our reflectance measurements were performed on a homogeneous bulk of glassy carbon sample. Pluchino et al. measured the scattered radiation by a single particle, small enough to be homogeneous. It is

Table 3.8. Results for index n and k obtained by the Kramers-Kronig method and by oscillator fit, in the case of glassy carbon.

The indices "OF" and "KK" stand for "Oscillator Fit" and "Kramers-Kronig," respectively.

	Wavelength (μm)						
	0.08	0.15	0.25	1.00	5.00	10.00	100.00
n_{OF}	1.03	1.46	1.40	1.95	2.97	2.88	5.91
n_{KK}	1.04	1.54	1.40	2.15	3.04	3.56	6.09
k_{OF}	0.91	0.38	0.56	0.70	1.15	1.91	5.26
k_{KK}	0.95	0.19	0.74	0.90	1.03	1.54	4.85

Table 3.9. n and k from this work and those of Taft and Phillip (1965) and Philipp (1977) at the same wavelengths.

	Wavelength (μm)							
	.1	.4	.5	.62	1.77	2	5	50
This work								
n	2.5	2.62	2.61	2.7	3.68	3.8	5.2	16
k	0.8	1.28	1.33	1.4	2.4	2.5	3.8	22
Taft and Philipp (1965) and Philipp (1977)								
n	2.4	2.52	2.54	2.6	3.78	3.9	5.1	15.8
k	0.75	1.35	1.36	1.46	2.49	2.6	4.0	22.8

strongly believed that the agreement of our results is due to the homogeneity of the materials on which the experiments were performed. To find optical constants of particles, many workers analyze reflectance data of particles pressed into pellets. Results obtained by this technique are rarely in good agreement for different samples. Chylek et al. (1981) argued that the differences are essentially due to the differing mass concentration of the particles. One reason we have chosen graphite and glassy carbon is because these materials are relatively homogeneous.

CHAPTER 4

SMALL PARTICLE EXTINCTION

This chapter deals with the extinction of small carbon particles. The production of the particles and their characterization are presented, and the sample preparation for the extinction measurements shown. Then the measurements leading to the mass calibration and to the extinction are described. Finally, results are presented and discussed.

Particle Production and Characterization

Graphite and three other types of carbon have been investigated. These powders are:

1. very fine graphite (Ashbury #250, Dixon),
2. standard lampblack,
3. particles (for solar energy absorption) produced by Hunt (1979) by acetylene pyrolysis at the Lawrence Berkeley Laboratory; those particles are referred to in this work as "LBL Smoke",
4. particles were made by evaporating carbon in an inert gas atmosphere.

The chamber in which these particles were made was evacuated to 2×10^{-4} torr with an oil diffusion pump. The

system was then purged with helium to reduce the partial pressure of oxygen, and reevacuated. Finally the chamber, isolated from the pumping system, was filled with helium, and an arc was struck between carbon electrodes (glassy carbon). The particles were collected on appropriate substrates.

The particles were observed with a "Scanning Electron Microscope" (SEM) and/or a "Transmission Electron Microscope" (TEM). For this purpose a small amount of "LBL Smoke," lampblack, or graphite powder was added to methane and the mixture dispersed ultrasonically. The cloudy liquid was then put in a syringe adapted to a Nucleopore membrane filter holder and filtered. The filter retained the individual particles with diameter larger than its pores and also chain-like aggregates of particles. Samples prepared with this technique were observed with the SEM. Results shown in Figs. 4.1 and 4.2 confirmed what is commongly observed: spherical shape for most carbon and plate-like shape for graphite (Walker, 1963). The nucleopores used had 0.25 μm diameter pores. Many of the particles presumably had smaller diameter than 0.25 μm.

Smoke made by arc evaporation of bulk glassy carbon was collected directly on grids for observation with TEM. Results showed that in this case, too, the particles are rather spherical, although not as perfect as observed for other particles (see Fig. 4.3). The heat generated by

Graphite (Dixon, HPN-2)

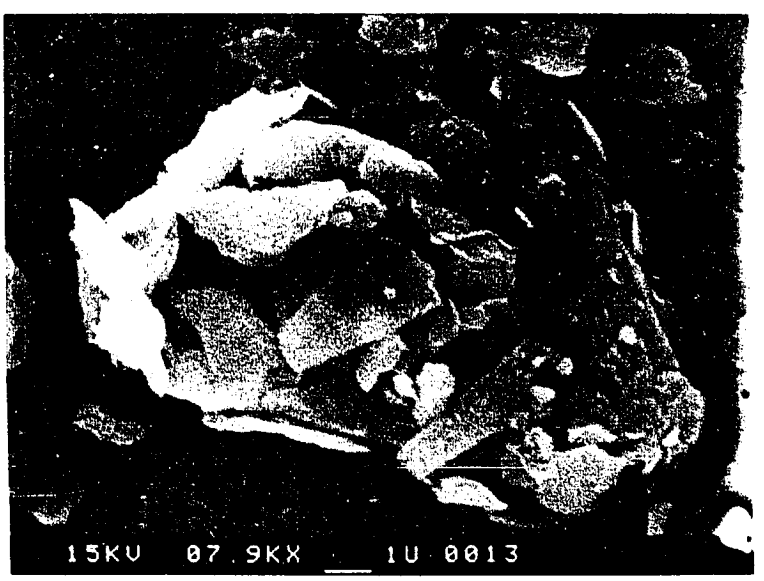

Graphite (Ashbury, Micro #250)

Fig. 4.1. Scanning electron microscope view of two types of graphite particles.

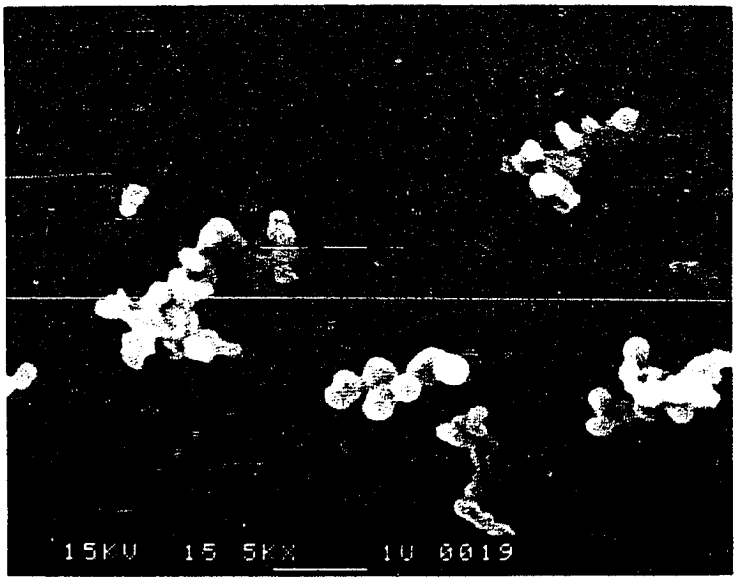

LBL Smoke particles

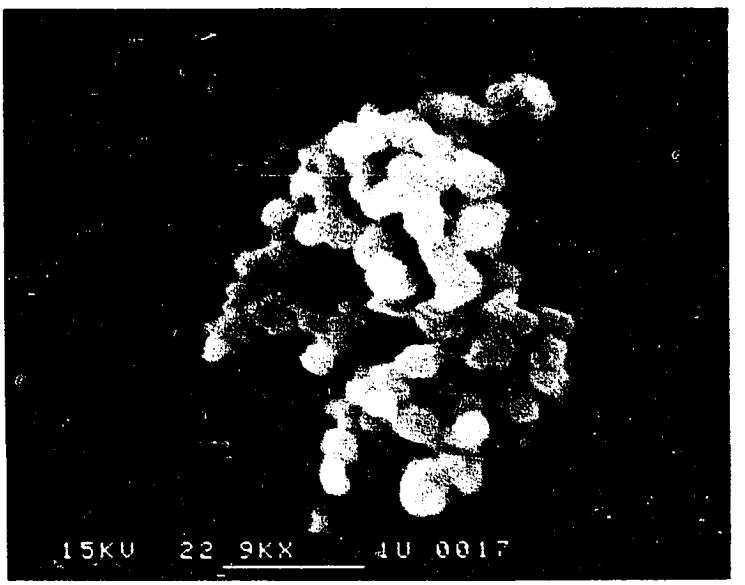

Lampblack particles

Fig. 4.2. Scanning electron microscope view of "LBL smoke" particles and lampblack particles.

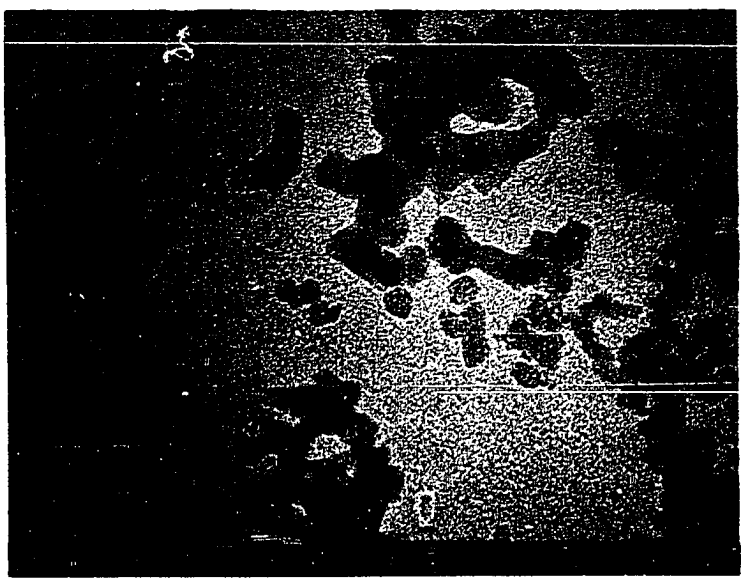

Fig. 4.3. Transmission electron microscope view of glassy carbon with magnification 250KX.

electrons striking the samples during the observation process is probably responsible for the ragged edges (Walker, 1963).

X-ray powder patterns and electron diffraction patterns observed in the transmission electron microscope showed diffuse bands with little distinction between "LBL smoke," lampblack, and glassy carbon smoke. In contrast, the graphite showed distinct diffraction patterns. It was concluded that the first three are mainly amorphous while the graphite is highly crystalline.

Sample Preparation

The transmission measurements from which the extinction was determined required suspension of the particle in one way or another. When they were collected on a usable substrate such as quartz or LiF, no further sample preparation was necessary; otherwise, special particle suspension techniques had to be used.

For extinction measurements from the visible to the mid IR, the KBr pellet technique was used. A small amount of the particulates (typically 50 to 200 μg) was mixed with 0.5 mg of IR quality of KBr in a vial that contained a small steel ball. The mixture was first hand shaken and then shaken for 5 to 10 minutes on a "Wig-L-Bug" dental amalgamator. The mixture was then transferred to an evacuable die connected to a vacuum-pumping system and placed on a

hydraulic press. After evacuating for about two minutes, pressure was applied and slowly increased up to about 2000 lbs per square inch. The vacuum was maintained for two more minutes, then released, as air was slowly admitted to the system. Finally, the pellet was carefully extracted.

For the far IR extinction measurements, polyethylene powder was used as the dispersion medium; 0.1 mg of polyethylene was used in each vial. In this case, shaking a vial caused the mixture to stick to its wall because of electrostatic forces. To circumvent this problem, acetone was added to the mixture. The vial was hand shaken, slightly warmed, and left open overnight to allow the acetone to evaporate. The mixture was then scraped off the container walls and transferred to the KBr die. The die was heated on a hot plate during its evacuation. A gentle hand pressure was exerted on the plunger of the die at the beginning of the heating. Still under evacuation, the die was removed from the hot plate and slowly cooled. The pellet was then carefully removed, with the help of a razor blade, and weighed. If m_1 is the mass of the polyethylene, m_2 the mass of the particles with which the sample preparation was started, and m_3 the mass of the pellet obtained, then:

$$m \simeq \left(\frac{m_2}{m_1}\right) m_3$$

is approximately the mass of particles in the pellet.

Measurements

The instruments used to acquire data have been described earlier (see Chapter 3). With the Cary 14, a zero-absorption trace was recorded with two identical sample holders in the two beams. The sample was then inserted in the front beam and a reference blank was placed in the back beam. The spectrophotometer recorded the optical density (OD) as a function of the wavelength. The measuring technique on the Perkin Elmer was the same as on the Cary 14, except that the zero and the 100% lines had to be recorded. The spectra obtained gave intensities which permitted the calculation of the transmission.

The Beckman 11 was used in a one-beam mode. The transmission through the sample and the reference blank was measured separately. The absorption of the particles was found from the ratio of the two transmissions. The calculations of volume-normalized extinction (α) requires knowledge of the mass density σ (mass/area) of the particles. For the pellets used in IR, the mass of particles suspended in a matrix was large enough for weighing with an analytical balance. In the UV, the absorption of carbon particles is so high that a very small quantity of particles must be used to get any transmission. In that case, it was practically impossible to weight the particles; an optical calibration method was used to find σ.

A sufficient quantity of carbon smoke was collected on glass slides and the optical densities (OD) measured in the visible. Each slide was weighed with and without the smoke. Knowing the mass m of the particles on a slide, and the area A of the substrate, $\sigma = m/A$ was computed. Optical density was plotted as a function of σ for several samples of varying thickness, as shown in Fig. 4.4. The curve shows a leveling off of OD with increasing σ, presumably due to the increasing effect of multiple scattering. In order to avoid the multiple scattering region, the slope of the linear curve at small σ is used to determine a calibration constant (OD/σ) at each wavelength. This calibration can then be used to determine mass densities from optical transmission measurements for samples that are too light for conventional weighing techniques. By calibrating the mass density in the near infrared and the visible, optical measurements on very light samples (i.e., 5 $\mu g/cm^2$) can be extended into the highly absorbing regions of the UV.

Results and Discussion

In this section, results of extinction measurements on graphite and amorphous carbon are presented and discussed with respect both to calculations and to other workers' results. This is done first for $\lambda > 0.4$ μm and then for $\lambda \leq 0.4$ μm.

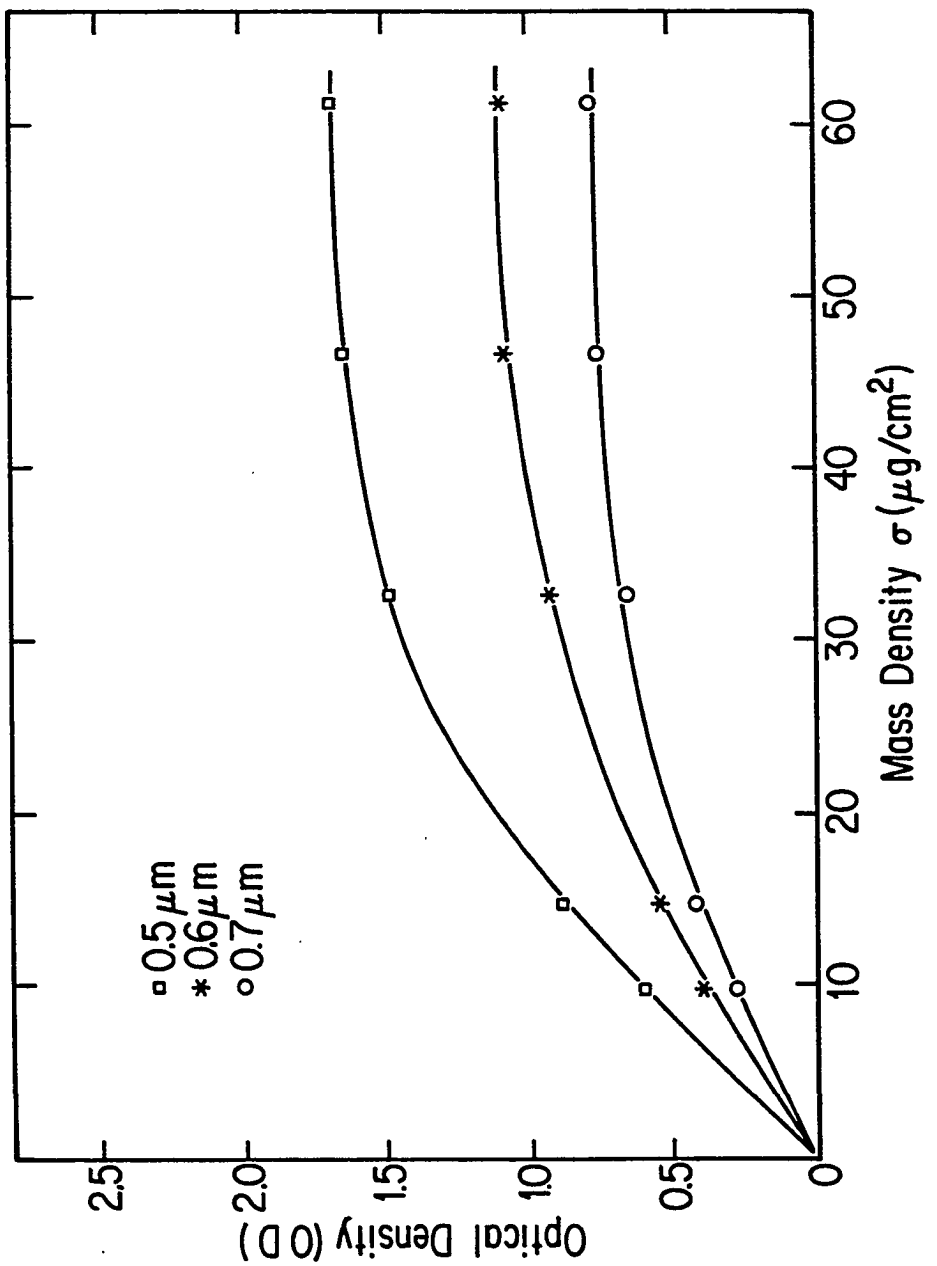

Fig. 4.4. Variation of the optical density (OD) of glassy carbon, as a function of the mass density σ at various wavelengths.

In Fig. 4.5 are plotted the extinction results from graphite powders (Ashbury micro #250, Dixon HPN-2). On the same figure are plotted two sets of calculations, one based on a continuous distribution of spheres (CS) theory and the other on a continuous distribution of ellipsoids (CDE).

Although some workers argued that bulk optical properties may not be appropriate for micron-sized particles (Pluchino et al., 1980), the calculations were done using optical constants derived in Chapter 3, with the assumption that the particles are large enough for bulk optical properties to be applicable. A discussion of this point can be found in the review by Huffman (1977, pp. 212-215).

A comparison of the two calculated results shows a substantial difference in strength of the extinction in the infrared region from about $\lambda \sim 1.0$ μm to 100 μm. This provides a quantitative illustration of how shape affects extinction of carbon particles in the infrared.

Visible and Infrared Range

Most of our studies on graphite were done on the Ashbury powder, which was available in large enough quantities to permit the preparation of many samples. Therefore, the discussion of graphite experimental results will be based on the Ashbury sample only.

Three sets of results were obtained (see Fig. 4.5). From $\lambda \sim 0.4$ μm to 25 μm, extinction of particles in KBr

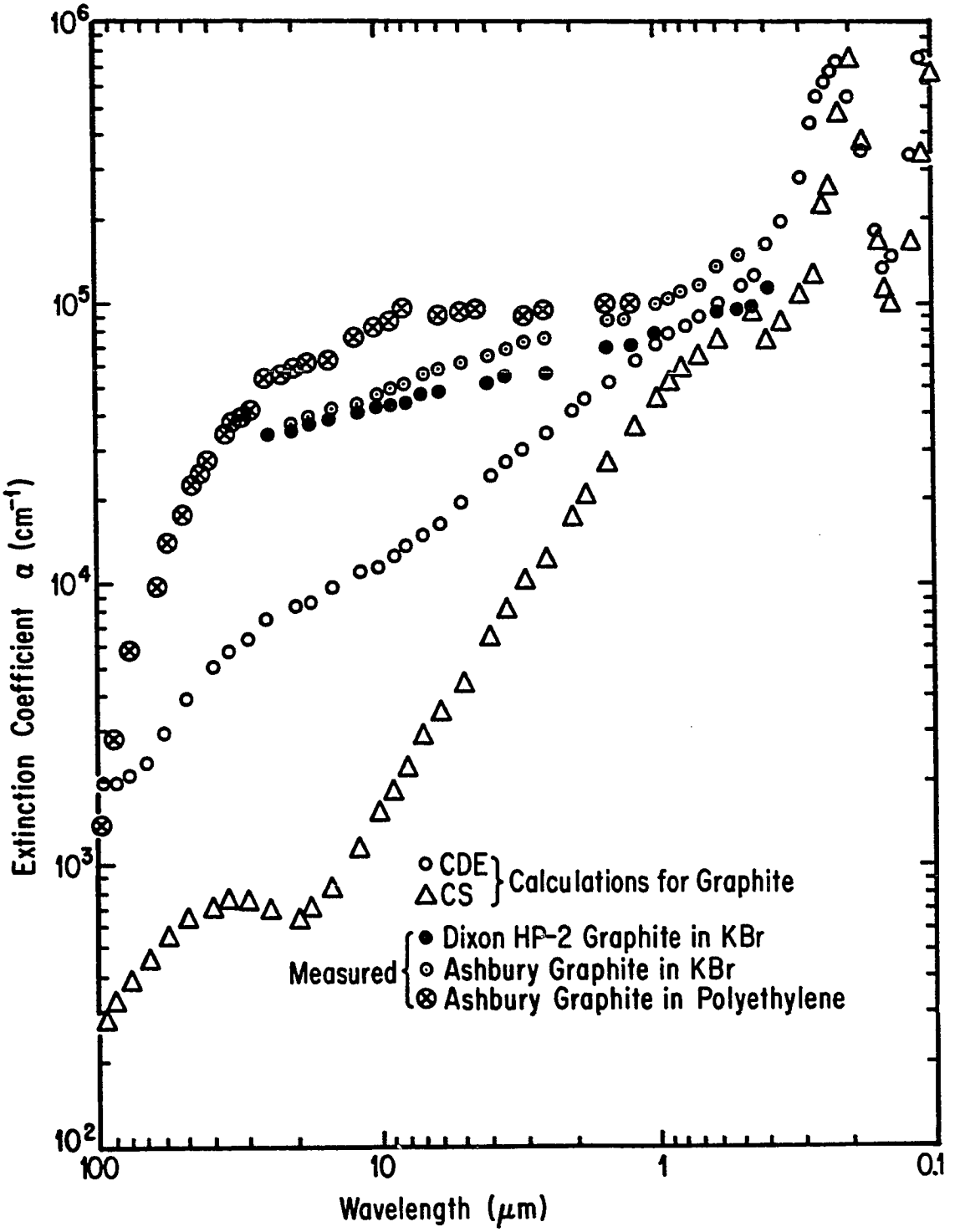

Fig. 4.5. Experimental extinction for graphite, compared to sphere theory (CS) and to CDE theory.

and extinction of particles in polyethylene are shown; above $\lambda \sim 25$ μm, extinction of particles in polyethylene only is presented. The polyethylene sample used from 0.4 μm to 25 μm was obtained from a pellet made by the technique described in the section on sample preparation, then thinned by exerting a slight pressure on the pellet placed between two microscope slides and heated. Comparison of the two results in the $\lambda \sim 0.4$ μm to 25 μm range shows differences which are due to the suspension media used. On the one hand, the carbon particles mixed well with the KBr powder during the vial shaking process; on the other, the polyehtylene and the particles stick to the wall of the vial when shaken, as previously explained.

The observed disagreement of theory and experiment is most likely due to the inappropriateness of the ellipsoid theory. Figure 4.1 provides evidence that the graphite particles are in fact plate-like particles.

The particle shape is probably responsible for the violation of the sum rule shown in Eq. (40). Indeed, in a very restricted wavelength range (i.e., 5 μm to 50 μm),

$$\int \alpha \, d\lambda \simeq 65 \quad ,$$

exceeding the maximum value which is 30.

Although this investigation was not planned as an illustration of the "shape effect," the comparison of experimental results to one another and to calculations has clearly shown the importance of the shape effect in extinctions.

Extinction of "LBL smoke" and lampblack was also investigated. Experimental results and calculations based on the same theories as for graphite are plotted in Fig. 4.6. Optical constants derived in Chapter 3 for glassy carbon have been used in the calculation. Extinction of fresh "LBL smoke" from $\lambda \sim 0.6$ μm to 15 μm is pratically the same as predicted by the sphere calculations. This is not surprising since Fig. 4.2 shows agglomerated spheres. These chains and clusters were probably dispersed in the shaking process.

Pellets made of "LBL smoke" were measured fresh and also two years later; they gave almost exactly the same results as new pellets made of two year old "LBL smoke." Because of the old pellet results, the increase in "LBL smoke" extinction has been assigned to a change in the optical constants of the particles, rather than to the shape effect. The nature of this change is not yet well understood; a graphitization hypothesis has been discounted because x-ray studies of the two-year-old particles did not show any sharp lines.

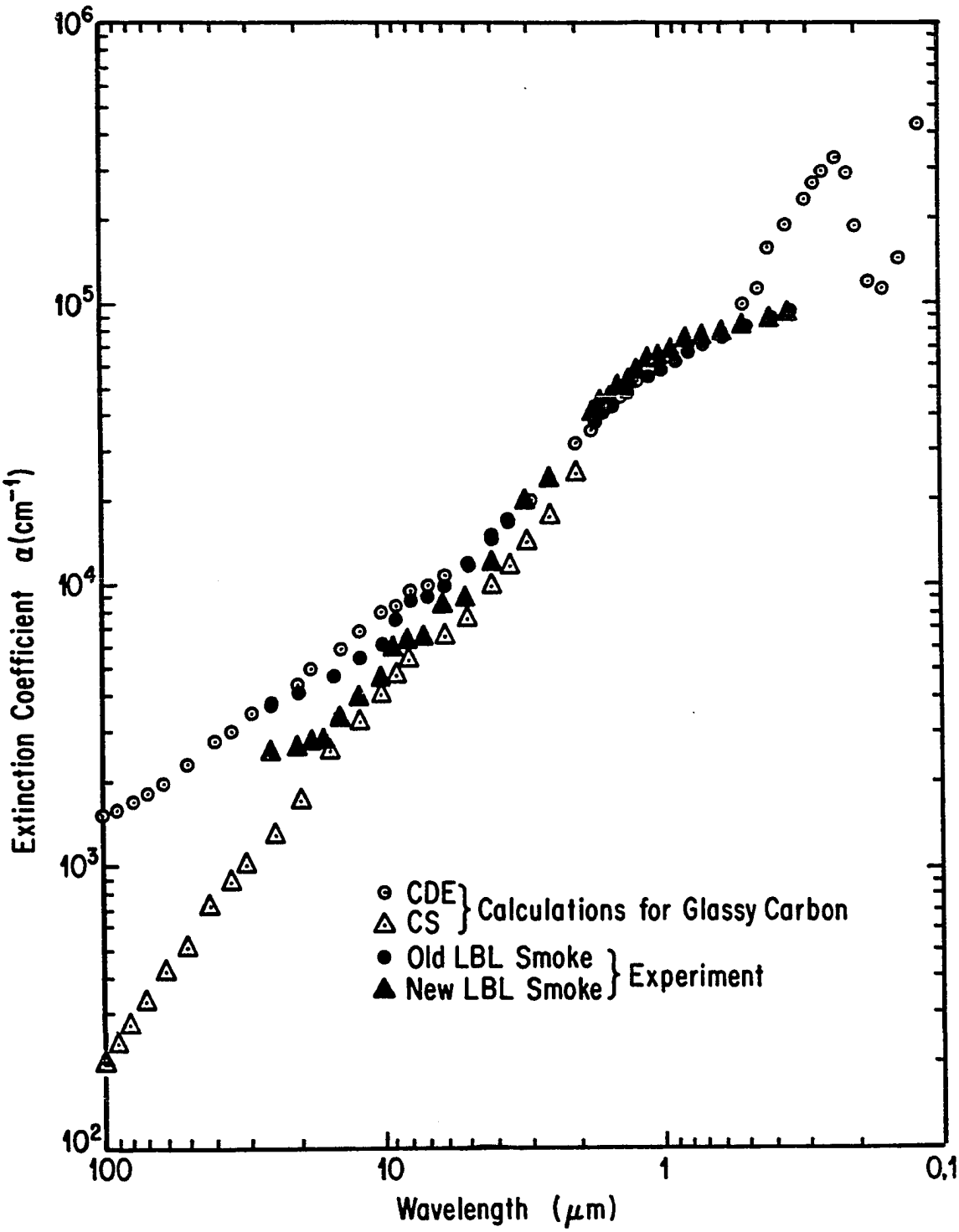

Fig. 4.6. Experimental extinction for "LBL smoke" with aging effect observed and comparison to sphere theory (CS) and to CDE theory.

Figure 4.7 shows that the lampblack extinction is higher than the highest "LBL smoke" extinction. The lampblack powder used might have experienced the same aging process as the "LBL smoke" and the difference in extinction might be due to a difference in the ages of the particles.

Koike, Hosegawa, and Manabe (1980) measured the extinction of arc evaporated graphite particles and particles produced by burning benzene and xylene in air. The measurements were performed from $\lambda \sim 0.21$ μm to 340 μm on samples prepared with the same techniques as ours. They found humps between $\lambda \sim 5$ μm and 15 μm (Koike et al., 1980). Our data confirmed the presence of these humps (see Figs. 4.5 and 4.6). Koike et al. also found a peak near $\lambda \sim 90$ μm. Neither the data of Blea et al. (1970) nor ours shows this peak. A broad peak found in our calculated result is located around $\lambda \sim 35$ μm and is more apparent in the sphere calculations than in the CDE case (see Fig. 4.5).

Blea et al. (1970) measured absorption coefficients of black polyethylene over a broad spectral range ($\lambda \sim 2.5$ μm to 3,300 μm). Although their scattered results were assigned to differences in grain size, mass concentration of carbon in polyethylene, and to the form of the carbon, our extinction results from one type of carbon to another are due to differences in the shapes of the particles.

Table 4.1 shows experimental results of this study and those of other workers at some specific wavelengths.

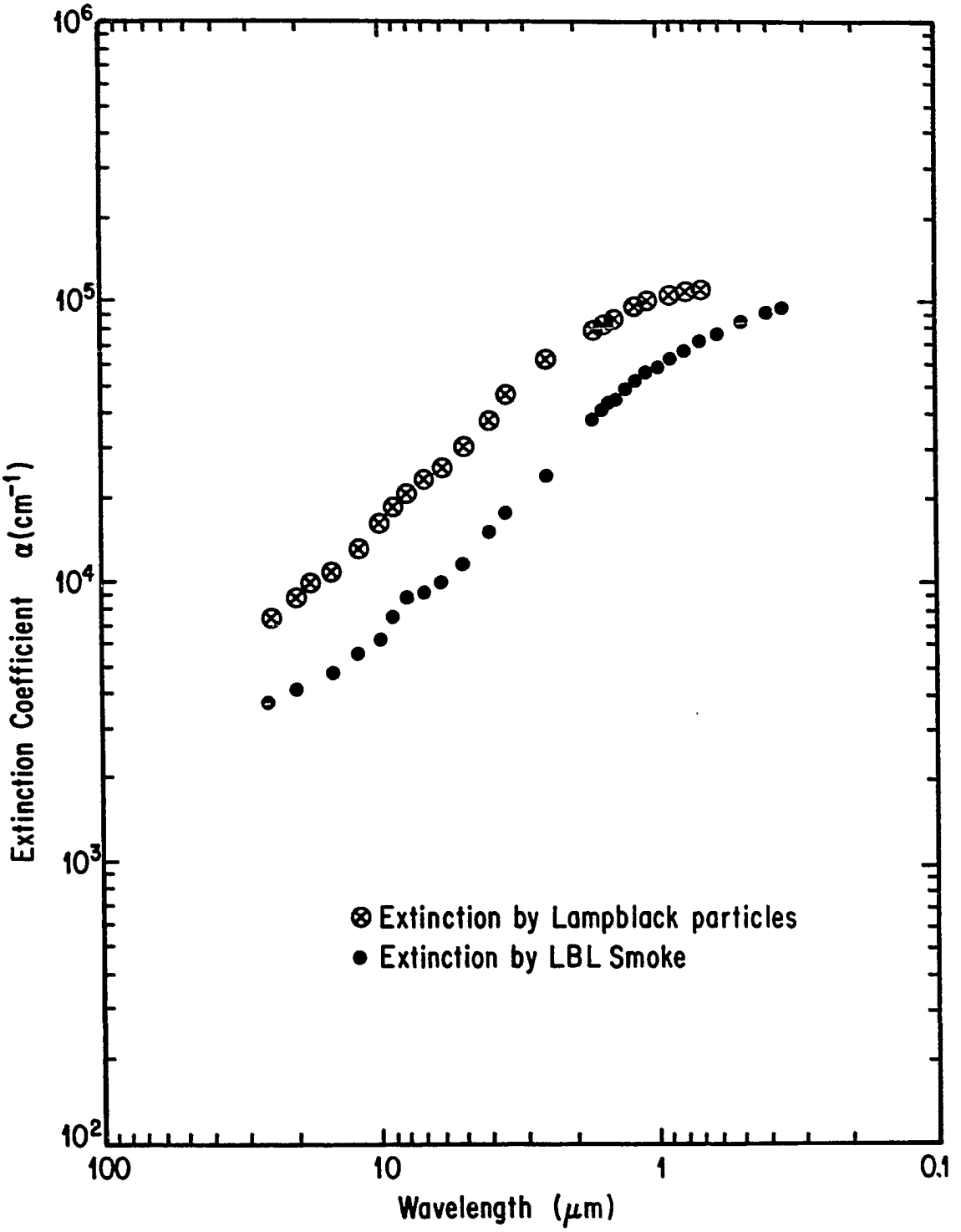

Fig. 4.7. Comparison of experimental extinctions by "LBL smoke" and by lampblack.

Table 4.1. Measured extinction coefficients at some wavelengths.

Authors	Samples	α (cm^{-1}) $\lambda \sim 0.5$ μm	$\lambda \sim 5$ μm	$\lambda \sim 10$ μm	Comments
This work	Ashbury Graphite #250	145×10^3	51×10^3	47×10^3	Particles in KBr
	LBL Smoke	83×10^3	11.5×10^3	6.2×10^3	Particles in KBr
Koike et al. (1980)	Arc evaporated graphite (TU)	225×10^3	22.5×10^3	15×10^3	
	Lampblack from benzene (BE)	188×10^3	15×10^3	8.25×10^3	Combustion in air
	Lampblack from xylene (XY)	112.5×10^3	8.25×10^3	6.0×10^3	Combustion in air
Blea et al. (1970)	USIC			22.5×10^3	Black polyethylene
	DOW		$\sim 24 \times 10^3$	15×10^3	

Ultraviolet Range

For short wavelengths the Rayleigh approximation, on which the sphere and CDE calculations are based, is hardly valid. A switch to Mie calculations is then necessary. Although the particles are not individual spheres or spherical at all (graphite), the calculations can give a rough basis for the evaluation of the experimental results.

Experimental results and calculations are shown in Figs. 4.8 and 4.9 for Ashbury graphite and glassy carbon, respectively. It might be surprising that the glassy carbon extinction peak is higher than the graphite one. It has been shown (Rathmann, 1981; Foxvog and Roessler, 1978) that the extinction out of the Rayleigh limit range is radius dependent, and that very fine particles have a higher peak. The graphite used was acquired as a finished powder with rather large particle sizes. The glassy carbon particles were arc-evaporated in helium atmosphere, a technique known for producing very fine particles (Rathmann, 1981). Also the particles were lightly deposited on the substrate to limit their agglomeration.

The graphite particles might obey some kind of sum rule by which the loss of strength in extinction observed between $\lambda = 0.22$ μm and 0.24 μm is compensated by the high extinction in the infrared region.

The strength of the experimentally found peak for glassy carbon is rather close to the peak calculated by

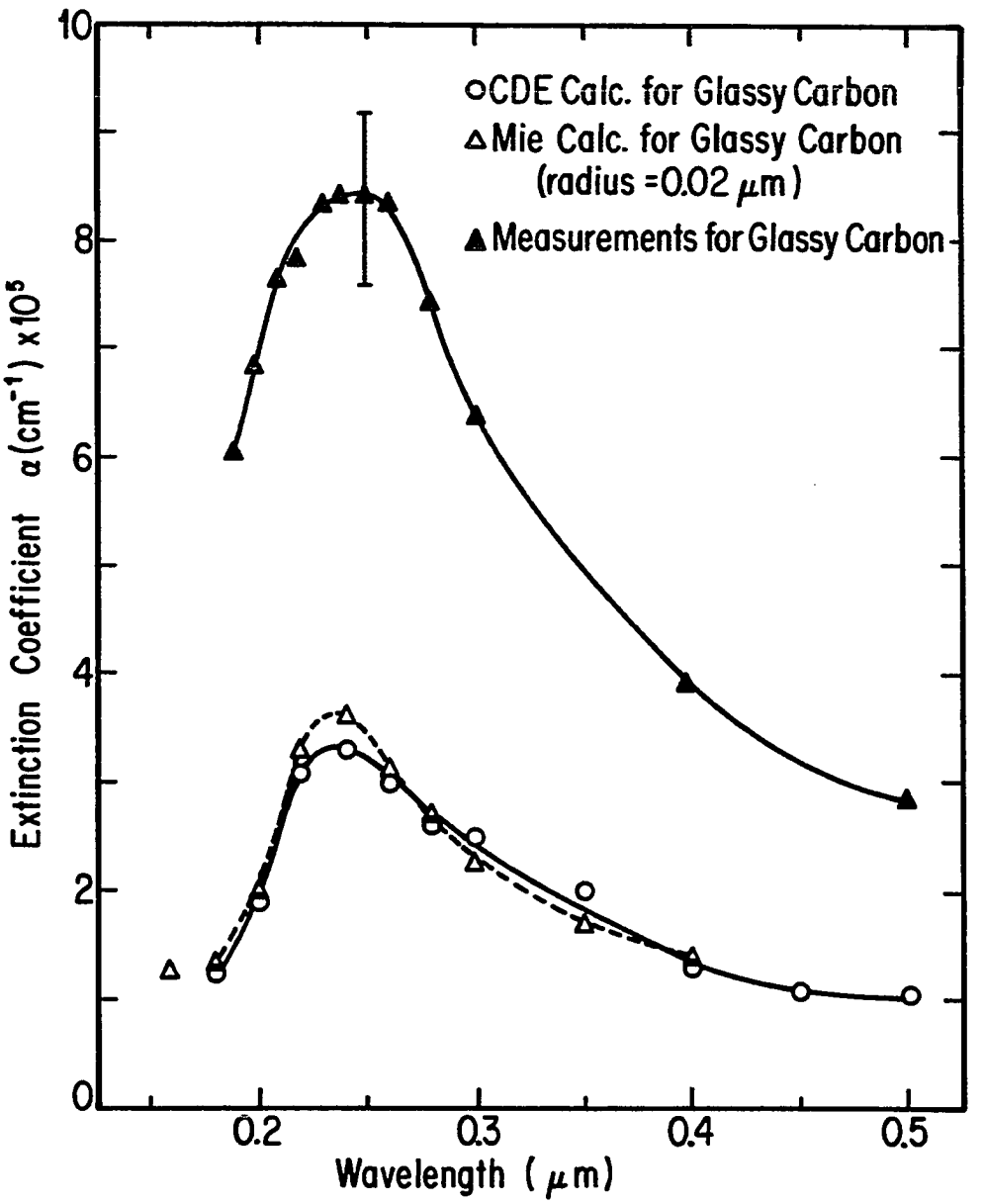

Fig. 4.8. Comparison of experimental extinction to calculated extinctions for glassy carbon around $\lambda \sim 0.22$ μm.

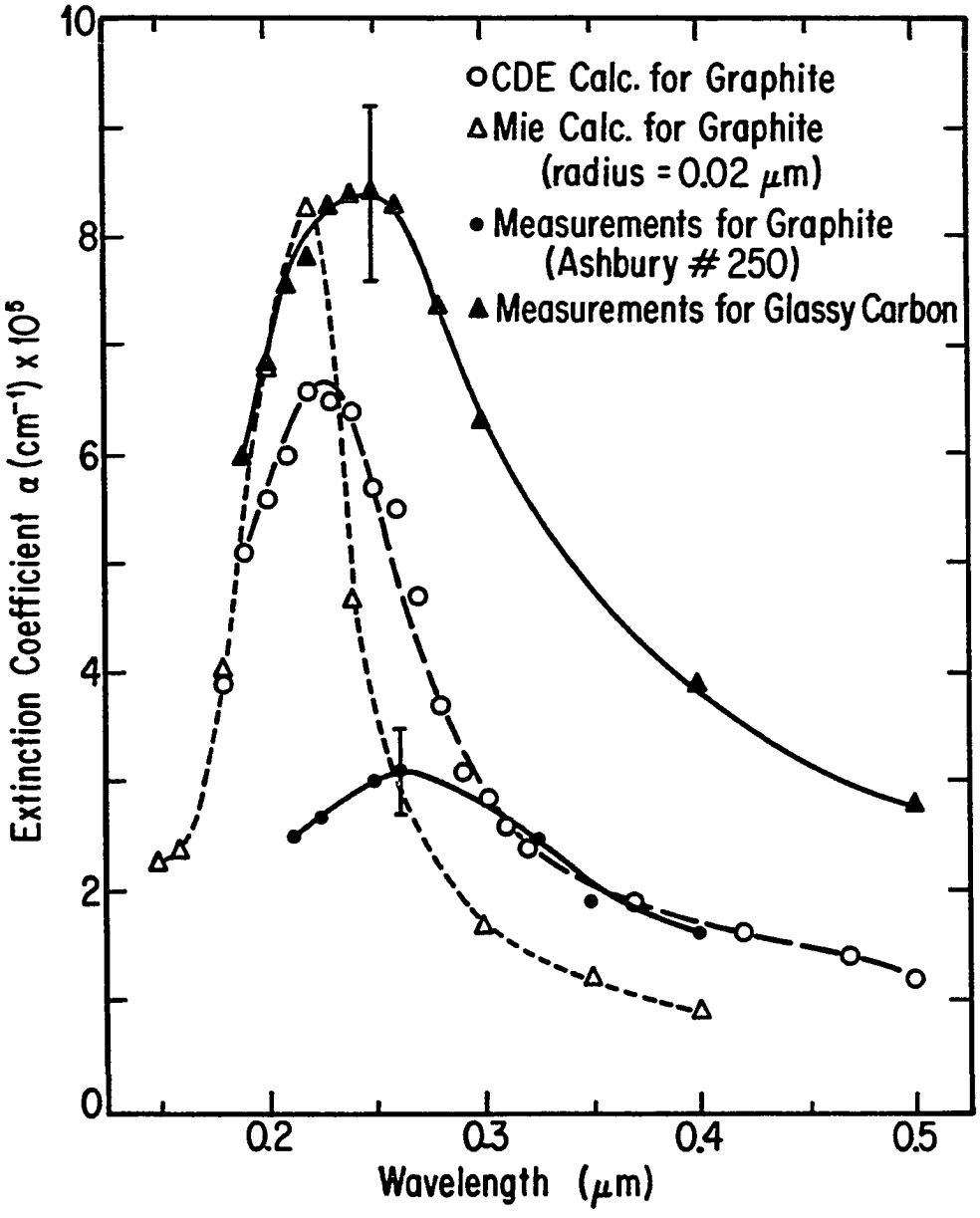

Fig. 4.9. Comparison of experimental extinctions for graphite and glassy carbon to calculated extinctions for graphite around $\lambda \sim 0.22$ μm.

by the Mie method for graphite (see Fig. 4.9). Although it is known that glassy carbon cannot be significantly altered by heat treatment (Halpin and Jenkins, 1969), the strength of the peak is a good basis for arguing that the particles have graphitized in their production process.

CHAPTER 5

SUMMARY AND CONCLUSION

Reflectance data for graphite for the E $\perp$ C orientation and for glassy carbon were compiled from the literature and augmented by our own measurements and/or extrapolations. They were analyzed by the use of the Kramers-Kronig method to yield consistent optical constants over a wide spectral range. For glassy carbon, our results are, at this writing, the only ones available beyond $\lambda \sim 10$ μm.

It was also shown that the homogeneity of the material on which measurements (reflectance, extinction, etc.) are performed is an important factor in obtaining dependable results.

Optical constants obtained for graphite for the E // C orientation by optical and by electron energy-loss methods over a broad (0.05 to 100 μm) spectral range have been combined to give more realistic results than could be provided by each method separately.

Fitting the reflectance data of graphite and glassy carbon to a Drude-Lorentz model was complicated by the existence of interband transitions which increase the reflectance without showing sharp peaks. But except for

the case of the E $\perp$ C polarization of graphite, the difference between experiment and fit was unimportant because of low reflectances; good results were thus obtained with this method over the spectral range.

Differences exist between experimental and calculated extinctions by small carbon particles. High experimentally observed extinctions are either due to a shape effect as observed with graphite, or to an aging process as noticed with the other types of carbon particles. The preparation of small particles by arc evaporation of bulk glassy carbon tends to graphitize the particles, thus enhancing the extinction. This effect was observed around $\lambda \sim 0.22$ μm for particles which were nominally glassy carbon (see Fig. 4.9).

The poor agreement between experiment and calculations leads to the conclusion that current models are not adequate for predicting extinctions by small carbon particles over a large spectral range. However, the empirical results provided by this work should be useful in designing projects like the solar energy collector conceived by Hunt (1979).

More experimental work should be done in order to reconcile the optical constants for graphite for the E // C orientation, as measured by optical and electron energy-loss techniques. The aging process and the graphitization

of the particles observed in this work need to be studied further and quantified.

Progress in reconciling experimental and theoretical extinctions by small carbon particles will probably depend on how well changes in the particles are understood and incorporated in calculations; it will also depend on the existence of theories which can properly deal with the shape of the particles.

APPENDIX A

TABULATION OF THE OPTICAL CONSTANTS OF GRAPHITE AND GLASSY CARBON

Table A.1. Optical constants of graphite for the E ⊥ C polarization.

λ (μm)	N	K	λ (μm)	N	K
0.050	0.381	0.313	1.200	3.180	2.000
0.055	0.390	0.543	1.500	3.430	2.180
0.060	0.400	0.850	1.800	3.700	2.430
0.065	0.500	1.150	2.000	3.830	2.520
0.070	0.650	1.330	2.500	4.300	2.750
0.075	0.850	1.700	3.000	4.300	2.950
0.080	1.000	2.000	3.500	4.480	3.330
0.085	1.900	2.450	4.000	4.730	3.550
0.090	2.600	1.650	4.500	5.030	3.730
0.095	2.630	1.350	5.000	5.230	3.830
0.100	2.400	0.900	6.000	5.400	4.030
0.110	2.150	0.500	7.000	5.400	4.450
0.120	1.900	0.130	8.000	5.700	4.950
0.125	1.700	0.100	9.000	5.980	5.250
0.140	1.470	0.130	10.000	6.100	5.550
0.150	1.100	0.160	12.000	6.140	6.850
0.160	0.980	0.280	15.000	6.250	8.000
0.180	0.830	0.650	18.000	6.550	9.000
0.200	0.800	1.200	20.000	6.750	11.000
0.220	0.850	2.000	25.000	7.500	13.000
0.240	1.200	2.400	30.000	8.500	15.500
0.250	1.600	2.450	35.000	10.000	18.500
0.260	2.100	2.650	40.000	11.500	20.500
0.270	2.550	2.450	50.000	16.500	23.500
0.300	2.700	1.700	60.000	20.700	22.000
0.350	2.620	1.360	70.000	22.500	19.300
0.400	2.610	1.240	80.000	21.500	18.900
0.450	2.600	1.250	90.000	20.000	18.800
0.500	2.600	1.370	100.000	18.300	21.300
0.600	2.700	1.360			
0.700	2.750	1.480			
0.800	2.850	1.630			
0.900	2.920	1.740			
1.000	3.000	1.800			

Table A.2. Optical constants of graphite for the E // C polarization.

λ (μm)	N	K	λ (μm)	N	K
0.050	0.980	0.360	1.200	1.400	0.100
0.055	0.950	0.420	1.500	1.400	0.100
0.060	0.850	0.480	1.800	1.470	0.100
0.065	0.800	0.600	2.000	1.500	0.100
0.070	0.790	0.780	2.500	1.600	0.150
0.075	0.833	0.833	3.000	1.730	0.150
0.080	0.940	0.950	3.500	1.860	0.150
0.085	0.960	1.05	4.000	1.960	0.150
0.090	1. 30	1.200	4.500	2.060	0.150
0.095	1.150	1.450	5.000	2.200	0.150
0.100	1.300	1.600	6.000	2.350	0.150
0.110	2.200	1.900	7.000	2.410	0.150
0.120	2.700	1.400	8.000	2.400	0.150
0.125	2.800	1.000	9.000	2.398	0.150
0.140	2.550	0.450	10.000	2.396	0.150
0.150	2.230	0.250	12.000	2.330	0.170
0.160	2.100	0.190	15.000	2.250	0.200
0.180	1.600	0.130	18.000	2.150	0.270
0.200	1.220	0.150	20.000	2.050	0.350
0.220	1.100	0.200	25.000	1.930	0.580
0.240	0.990	0.120	30.000	1.920	0.850
0.250	1.000	0.240	35.000	2.000	1.070
0.260	1.050	0.230	40.000	2.080	1.240
0.270	1.120	0.100	50.000	2.200	1.630
0.300	1.250	0.110	60.000	2.300	1.930
0.350	1.370	0.100	70.000	2.430	2.150
0.400	1.400	0.100	80.000	2.540	2.400
0.450	1.370	0.100	90.000	2.630	2.550
0.500	1.330	0.100	100.000	2.700	2.700
0.600	1.300	0.100			
0.700	1.300	0.100			
0.800	1.300	0.100			
0.900	1.300	0.100			
1.000	1.350	0.100			

Table A.3. Optical constants and extinction coefficients of graphite.

λ (μm)	$\varepsilon_{1//}$	$\varepsilon_{2//}$	$\varepsilon_{1\perp}$	$\varepsilon_{2\perp}$	$\alpha_{CS}(cm^{-1})$	$\alpha_{CDE}(cm^{-1})$
.050	.8308	.7056	.0472	.2385	.7359E+06	.9176E+06
.055	.7261	.7980	-.1427	.4235	.1139E+07	.1341E+07
.060	.4921	.8160	-.5625	.6800	.2062E+07	.1853E+07
.065	.2800	.9600	-1.0725	1.1500	.3511E+07	.2183E+07
.070	.0157	1.2324	-1.3464	1.7290	.3320E+07	.2244E+07
.075	0.0000	1.3878	-2.1675	2.8900	.2322E+07	.2312E+07
.080	-.0189	1.7860	-3.0000	4.0000	.1700E+07	.2318E+07
.085	-.1809	2.0160	-2.3925	9.3100	.1082E+07	.2035E+07
.090	-.379	2.4720	4.0375	8.5800	.9190E+06	.1407E+07
.095	-.7800	3.3350	5.0944	7.1010	.6044E+06	.1254E+07
.100	-.8700	4.1600	4.9500	4.3200	.6652E+06	.1028E+07
.110	1.2300	8.3600	4.3725	2.1500	.3413E+06	.7065E+06
.120	5.3300	7.5600	3.5931	.4940	.1563E+06	.3428E+06
.125	6.8400	5.6000	2.8800	.3400	.1200E+06	.2406E+06
.140	6.3000	2.2950	2.1440	.3822	.1011E+06	.1482E+06
.150	4.9104	1.1150	1.1644	.3520	.1148E+06	.1330E+06
.160	4.3739	.7980	.8820	.5488	.1730E+06	.1822E+06
.180	2.5431	.4160	.2664	1.0790	.3796E+06	.3454E+06
.200	1.4659	.3660	-.8000	1.9200	.7344E+06	.5535E+06
.220	1.170	.4400	-3.2775	3.4000	.4785E+06	.7322E+06
.240	.9657	.2376	-4.3200	5.7600	.2557E+06	.6625E+06
.250	.9424	.4800	-3.4425	7.8400	.2268E+06	.5944E+06
.260	1.0496	.4830	-2.6125	11.1300	.1666E+06	.5377E+06
.270	1.2444	.2240	.5000	12.4950	.1222E+06	.4257E+06
.300	1.5504	.2750	4.4000	9.1800	.1057E+06	.2770E+06
.350	1.8669	.2740	5.0148	7.1264	.8658E+05	.1983E+06
.400	1.9500	.2800	5.2745	6.4728	.7275E+05	.1603E+06
.450	1.8669	.2740	5.1975	6.5300	.9908E+05	.1224E+06
.500	1.7589	.2660	4.8831	7.1240	.9554E+05	.1201E+06
.600	1.680	.2600	5.3856	7.4520	.7552E+05	.9906E+05
.700	1.6800	.2600	5.3721	8.1400	.6609E+05	.8973E+05

Table A.3. Optical constants and extinction coefficients of graphite (continued).

λ (μm)	$\varepsilon_{1//}$	$\varepsilon_{2//}$	$\varepsilon_{1\perp}$	$\varepsilon_{2\perp}$	$\alpha_{CS}(cm^{-1})$	$\alpha_{CDE}(cm^{-1})$
.800	1.6800	.2600	5.4656	9.2910	.5830E+05	.8409E+05
.900	1.6800	.2600	5.4988	10.1616	.5182E+05	.7625E+05
1.000	1.8125	.2700	5.7600	10.8000	.4548E+05	.7150E+05
1.200	1.9500	.2800	6.1124	12.7200	.3626E+05	.6329E+05
1.500	1.9500	.2800	7.0125	14.9548	.2649E+05	.5227E+05
1.800	2.1509	.2940	7.7651	17.9820	.2011E+05	.4572E+05
2.000	2.2400	.3000	8.3185	19.3032	.1723E+05	.4157E+05
2.500	2.5375	.4300	10.9275	23.6500	.1209E+05	.3386E+05
3.000	2.9704	.5190	9.7875	25.3700	.1011E+05	.2988E+05
3.500	3.4371	.5580	8.9815	29.8368	.8095E+04	.2754E+05
4.000	3.8191	.5880	9.7704	33.5830	.6472E+04	.2492E+05
4.500	4.2211	.6180	11.3880	37.5238	.5203E+04	.2180E+05
5.000	4.8175	.6600	12.6840	40.0618	.4371E+04	.1953E+05
6.000	5.5000	.7050	12.9191	43.5240	.3414E+04	.1659E+05
7.000	5.7856	.7230	9.3575	48.0600	.2836E+04	.1536E+05
8.000	5.7375	.7200	7.9875	56.4300	.2226E+04	.1409E+05
9.000	5.7279	.7194	8.1979	62.7900	.1819E+04	.1270E+05
10.000	5.7183	.7188	6.4075	67.7100	.1555E+04	.1176E+05
12.000	5.4000	.7922	-9.2229	84.1180	.1147E+04	.1133E+05
15.000	5.0225	.9000	-24.9375	100.0000	.8307E+03	.9938E+04
18.000	4.5496	1.1610	-38.0975	117.9000	.6990E+03	.8756E+04
20.000	4.0800	1.4350	-75.4375	148.5000	.6323E+03	.8715E+04
25.000	3.3885	2.2388	-112.7500	195.0000	.6926E+03	.7453E+04
30.000	2.9639	3.2640	-168.0000	263.5000	.7743E+03	.6573E+04
35.000	2.855	4.2800	-242.2500	370.0000	.7648E+03	.5825E+04
40.000	2.7888	5.1584	-288.0000	471.5000	.7223E+03	.5128E+04
50.000	2.183	7.1720	-280.0000	775.5000	.6580E+03	.3929E+04
60.000	1.5651	8.8780	-55.5100	910.8000	.5649E+03	.2966E+04

Table A.3. Optical constants and extinction coefficients of graphite (continued).

λ (μm)	$\varepsilon_{1\parallel}$	$\varepsilon_{2\parallel}$	$\varepsilon_{1\perp}$	$\varepsilon_{2\perp}$	α_{CS} (cm^{-1})	α_{CDE} (cm^{-1})
70.000	1.2824	10.4490	133.7600	868.5000	.4640E+03	.2329E+04
80.000	.6916	12.1920	105.0400	812.7000	.3871E+03	.2105E+04
90.000	.4144	13.4130	46.5600	752.0000	.3279E+03	.1950E+04
100.000	0.0000	14.5800	-118.8000	779.5800	.2813E+03	.1951E+04

Table A.4. Optical constants and extinction coefficients of glassy carbon.

λ (μm)	ε_1	ε_2	N	K	α_{CS} (cm^{-1})	α_{CDE} (cm^{-1})
.040	.6932	.1808	.8395	.1077	.3509E+06	.3563E+06
.050	.5189	.2629	.7418	.1772	.4636E+06	.4832E+06
.060	.3323	.5240	.6902	.3796	.8643E+06	.8811E+06
.070	.1395	.9994	.7578	.6594	.1443E+07	.1290E+07
.080	.0558	1.6843	.9330	.9026	.1686E+07	.1433E+07
.090	.7043	2.3895	1.2640	.9452	.1153E+07	.1176E+07
.100	1.6324	2.5728	1.5296	.8410	.7343E+06	.8641E+06
.120	2.7261	1.9411	1.7425	.5570	.3504E+06	.4498E+06
.140	2.8390	.6859	1.6970	.2021	.1160E+06	.1431E+06
.160	1.8971	.4179	1.3856	.1508	.9614E+05	.1037E+06
.180	1.5109	.4472	1.2423	.1800	.1122E+06	.1156E+06
.200	1.3798	.7826	1.2178	.3213	.1838E+06	.1870E+06
.220	1.0962	1.3517	1.1909	.5675	.3044E+06	.3017E+06
.240	1.2475	1.9815	1.3396	.7396	.3226E+06	.3397E+06
.260	1.5744	2.1581	1.4570	.7406	.2692E+06	.3014E+06
.280	1.8439	2.2652	1.5435	.7338	.2298E+06	.2694E+06
.300	2.0453	2.2914	1.5995	.7163	.1998E+06	.2411E+06
.350	2.4116	2.3585	1.7007	.6934	.1523E+06	.1937E+06
.400	2.6026	2.3424	1.7470	.6704	.1242E+06	.1615E+06
.450	2.7388	2.3957	1.7857	.6706	.1148E+06	.1132E+06
.500	2.8268	2.4851	1.8153	.6845	.1044E+06	.1036E+06
.600	3.0359	2.6605	1.8805	.7074	.8777E+05	.8821E+05
.700	3.1521	2.9959	1.9366	.7735	.8042E+05	.8173E+05
.800	3.3749	3.1929	2.0026	.7972	.7033E+05	.7268E+05
.900	3.4084	3.4466	2.0317	.8482	.6557E+05	.6828E+05
.920	3.4229	3.5226	2.0414	.8628	.6493E+05	.6779E+05
.940	3.4242	3.5753	2.0463	.8736	.6418E+05	.6709E+05
.960	3.4615	3.6481	2.0604	.8853	.6322E+05	.6636E+05
.980	3.4258	3.7080	2.0584	.9007	.6306E+05	.6615E+05

Table A.4. Optical constants and extinction coefficients of glassy carbon (continued).

λ (μm)	ε_1	ε_2	N	K	α_{CS} (cm^{-1})	α_{CDE} (cm^{-1})
1.000	3.6452	3.8023	2.1110	.9006	.6014E+05	.6406E+05
1.200	4.1298	4.2824	2.2449	.9538	.4932E+05	.5484E+05
1.400	4.7151	4.6160	2.3784	.9704	.3992E+05	.4644E+05
1.600	5.0430	4.8707	2.4650	.9920	.3416E+05	.4085E+05
1.800	5.4801	5.1030	2.5464	1.0020	.2911E+05	.3596E+05
2.000	5.8491	5.3733	2.6260	1.0231	.2552E+05	.3248E+05
2.500	6.8442	5.6166	2.8016	1.0024	.1815E+05	.2456E+05
3.000	7.2297	5.6681	2.8650	.9892	.1442E+05	.1994E+05
3.500	7.7058	5.9387	2.9525	1.0057	.1194E+05	.1707E+05
4.000	8.1025	6.2812	3.0294	1.0367	.1028E+05	.1515E+05
4.500	8.2643	6.1868	3.0486	1.0147	.8863E+04	.1314E+05
5.000	8.1530	6.2523	3.0354	1.0299	.8140E+04	.1203E+05
6.000	8.5799	7.2198	3.1459	1.1475	.7000E+04	.1090E+05
7.000	8.3985	7.9049	3.1569	1.2520	.6407E+04	.1015E+05
8.000	9.2497	9.4969	3.3546	1.4135	.5529E+04	.9624E+04
9.000	9.5522	10.0839	3.4236	1.4727	.4868E+04	.8774E+04
10.000	10.2428	10.9611	3.5528	1.5426	.4220E+04	.8063E+04
11.000	10.6000	11.6268	3.6286	1.6021	.3777E+04	.7499E+04
12.000	11.0701	12.0562	3.7039	1.6275	.3357E+04	.6887E+04
13.000	11.2024	12.6858	3.7501	1.6914	.3097E+04	.6543E+04
14.000	11.7419	13.4148	3.8451	1.7444	.2786E+04	.6156E+04
15.000	11.8934	13.8275	3.8815	1.7812	.2579E+04	.5826E+04
16.000	12.2703	14.4811	3.9529	1.8317	.2366E+04	.5543E+04
17.000	12.3656	15.1316	3.9942	1.8942	.2217E+04	.5349E+04
18.000	13.0275	15.9965	4.1023	1.9497	.2011E+04	.5101E+04
19.000	13.3052	16.1471	4.1369	1.9516	.1856E+04	.4813E+04
20.000	13.5307	16.5243	4.1766	1.9782	.1745E+04	.4603E+04
21.000	13.6685	17.1490	4.2189	2.0324	.1644E+04	.4469E+04
23.000	14.2323	17.9435	4.3090	2.0821	.1441E+04	.4119E+04
25.000	14.2397	19.1165	4.3633	2.1906	.1308E+04	.3945E+04

Table A.4. Optical constants and extinction coefficients of glassy carbon (continued).

λ (μm)	ε_1	ε_2	N	K	α_{CS} (cm^{-1})	α_{CDE} (cm^{-1})
27.000	14.7927	20.2703	4.4658	2.2695	.1241E+04	.3684E+04
29.000	14.9539	21.5445	4.5376	2.3740	.1141E+04	.3535E+04
31.000	15.4345	22.3080	4.6131	2.4179	.1041E+04	.3325E+04
33.000	15.4153	23.5677	4.6678	2.5245	.9716E+03	.3222E+04
35.000	16.0055	24.7082	4.7668	2.5917	.8871E+03	.3066E+04
37.000	16.1425	25.7730	4.8246	2.6710	.8277E+03	.2955E+04
39.000	16.6553	26.7136	4.9059	2.7226	.7644E+03	.2819E+04
41.000	16.7579	27.8682	4.9637	2.8072	.7171E+03	.2734E+04
43.000	17.2855	28.7237	5.0403	2.8494	.6662E+03	.2613E+04
45.000	17.5537	29.7916	5.1059	2.9176	.6247E+03	.2527E+04
50.000	18.5925	31.4865	5.2516	2.9978	.5356E+03	.2284E+04
55.000	18.2377	33.8666	5.3240	3.1802	.4800E+03	.2167E+04
60.000	18.7027	36.0256	5.4449	3.3082	.4242E+03	.2024E+04
65.000	17.8914	38.4061	5.4891	3.4984	.3879E+03	.1950E+04
70.000	18.4942	41.9212	5.6707	3.6963	.3400E+03	.1850E+04
75.000	18.1405	43.4166	5.7094	3.8022	.3134E+03	.1766E+04
80.000	18.2833	46.7814	5.8528	3.9965	.2804E+03	.1697E+04
85.000	17.6025	48.9788	5.9012	4.1499	.2592E+03	.1639E+04
90.000	17.3795	51.4302	5.9861	4.2958	.2376E+03	.1577E+04
95.000	15.2082	53.2932	5.9426	4.4840	.2257E+03	.1555E+04
100.000	17.3215	60.8160	6.3465	4.7913	.1893E+03	.1491E+04
105.000	22.4760	64.7425	6.7457	4.7988	.1628E+03	.1363E+04
205.000	43.9262	119.5903	9.2555	6.4605	.4555E+02	.7094E+03
305.000	37.6603	167.3121	10.2264	8.1604	.2396E+02	.5341E+03
405.000	51.2939	222.4011	11.8223	9.4060	.1358E+02	.4039E+03
505.000	54.4501	241.3914	12.2863	9.8236	.1007E+02	.3257E+03
605.000	46.7167	311.0457	13.4397	11.5719	.6728E+01	.2882E+03
705.000	44.1477	352.5256	14.1320	12.4726	.5135E+01	.2522E+03
805.000	49.8105	403.6371	15.1081	13.3563	.3931E+01	.2216E+03
905.000	73.5612	470.0931	16.5737	14.1619	.2975E+01	.1932E+03

SELECTED BIBLIOGRAPHY

Abdelrhaman, M., Fumeaux, P., and Suter, P., Solar Energy 22, 45 (1979).

Arakawa, E. T., Williams, M. W., and Inagaki, T., J. Appl. Phys. 48, 3176 (1977).

Blea, J. M., Parks, W. F., Ade, P. A. R., and Bell, R. J., J. Opt. Soc. Am. 60, 603 (1970).

Bohren, C. F., and Huffman, D. R., Absorption and Scattering of Light by Small Particles (New York: John Wiley, 1983).

Carter, J. G., Huebner, R. H., Ham, R. N., and Birkhoff, R. D., Phys. Rev. 137A, 639 (1965).

Chylek, P., Ramaswany, V., Cheng, R., and Pinnick, R. G., Appl. Optics 20, 2980 (1981).

Dalzell, W. H., and Sarofin, A. F., J. Heat Transf. 91, 100 (1969).

Daniels, J., Festenberg, C. V., Raether, H., and Zeppenfeld, K., Springer Tracts in Mod. Phys. 54, 77 (1970).

Day, K. L., and Huffman, D. R., Nature 243, 50 (1973).

Debye, P., Annln. Phys. 30, 59 (1909).

Decker, D., Ph.D. Dissertation, University of California, Riverside (1969).

DiNardo, R. P., and Goland, A. N., J. Opt. Soc. Am. 61, 1321 (1971).

Ergun, S., Nature 213, 135 (1967).

Faxvog, F. R., and Roessler, D. R., Appl. Optics 16, 2612 (1978).

Foster, P. J., and Howarth, C. R., Carbon 6, 719 (1968).

Gouw, T. H., Guide to Modern Methods of Instrumental Analysis (New York: John Wiley, 1972).

Greenaway, D. L., Harbeke, G., Bassani, F., and Tossati, E., Phys. Rev. 178, 1340 (1969).

Hagemann, H. J., Gudat, W., and Kuntz, C., Deutsches Electronen-Synchrotron DESY SR-74/7 (1974).

Halpin, M. K., and Jenkins, G. M., Proc. Roy. Soc. Lond. A 313, 421 (1969).

Howarth, C. R., Foster, P. J., and Thring, M. W., Proceeding of the Third Int. Heat Transf. Conference 5, 122 (1966).

Huffman, D. R., Department of Physics, University of Arizona, Tucson, private communication (1979).

_____, Adv. in Phys. 26, 129 (1977).

_____, Astr. and Space Sci. 34, 175 (1975).

Huffman, D. R., and Bohren, C. F., in Light Scattering by Irregularly Shaped Particles, D. W. Shuerman, ed. (New York: Plenum Press, 1980).

Hunt, A. J., in Topical Meeting on Optical Phenomena Peculiar to Matter of Small Dimensions, Opt. Soc. of America (1980).

_____, in Proceeding of the 13th Intersociety Energy Conversion Engineering Conference, Boston, MA, Aug. 5-10 (1979).

_____, Small Particle Heat Exchangers, Lawrence Berkeley Laboratory Report LBL 7841 (1978).

Jackson, J. D., Classical Electrodynamics, 2nd ed. (New York: John Wiley, 1975).

Janzen, J., J. Coll. Inter. Sci. 69, 436 (1979).

Kerker, M., The Scattering of Light and Other Electromagnetic Radiations (New York: Academic Press, 1969).

Kittel, C., Introduction to Solid State Physics, 5th ed. (New York: John Wiley, 1976).

Klucker, R., Thesis, University of Munich (1971).

Klucker, R., Skibowski, M., and Steinman, W., Phys. Stat. Sol. (B) 65, 703 (1974).

Koike, C., Hasegawa, H., and Manabe, A., Astr. and Space Sci. 67, 495 (1980).

Lee, S. C., and Tien, C. L., in Eighteen International Symposium on Combustion, The Combustion Institute (1981).

Lefevre, J., Astro. Astrophys. 5, 37 (1970).

Lehnam, A. P., and Treherne, D. M., The Observatory 86, 36 (1966).

Mallett, C. P., Phys. C: Solid State Phys. 14, L213 (1981).

Mie, G., Annln. Phys. 25, 377 (1908).

Miller, R. G., Laboratory Methods in Infrared Spectroscopy (London: Heyden, 1972).

National Academy of Sciences, Understanding Climatic Change, A Program for Action (Washington, DC: NAS, 1975).

Philipp, H. R., Phys. Rev. 16B, 2896 (1977).

Pluchino, A. B., Goldberg, S. S., Dowling, J. M., and Randal, C. M., Appl. Optics 19, 3370 (1980).

Purcell, E. M., Astrophys. J. 158, 433 (1969).

Rathmann, J., Ph.D. Dissertation, University of Arizona, Tucson (1981).

Sato, Y., J. Phys. Soc. Jpn. 24, 489 (1968).

Shobert II, E. I., in Modern Materials, Vol. 4, B. W. Gouser and H. H. Hausner, eds. (New York: Academic Press, 1964).

Steyer, T. R., Ph.D. Dissertation, University of Arizona, Tucson (1974).

Stull, V. R., and Plass, G., J. Opt. Soc. Am. 50, 121 (1960).

Taft, E. A., and Philipp, H. R., Phys. Rev. 138A, 197 (1965).

Tomaselli, V. P., Rivera, R., Edewaard, D. C., and Möller, K. D., Appl. Optics 20, 396 (1981).

Tossati, E., and Bassani, F., Nuovo Cimento 65B, 161 (1970).

Twitty, J. T., and Weiman, J. A., J. Appl. Meteo. 10, 725 (1971).

Twomey, S., and Huffman, D. R., in Light Absorption by Aerosol Particles (Hampton, VA: Spectrum Press, 1982).

van de Hulst, H. C., Light Scattering by Small Particles (New York: John Wiley, 1957).

Venghaus, H., Phys. Stat. Sol. (B) 71, 609 (1975).

_____, Phys. Stat. Sol. (B) 81, 221 (1977).

Walker, P. L., Jr., in Ultrafine Particles, W. E. Kuhn, ed. (New York: John Wiley, 1963).

Wickramasinghe, N. C., Light Scattering Functions for Small Particles (London: Adam Hilger, 1973).

Williams, M. W., and Arakawa, E. T., J. Appl. Phys. 43, 3460 (1972).

Wooten, F., Optical Properties of Solids (New York: Academic Press, 1972).

Zeppenfeld, K., Phys. Lett. 25A, 335 (1967).

Ziman, J. M., Principles of the Theory of Solids (Cambridge: Cambridge University Press, 1969).